Atmos. Meas. Tech. Discuss., 7, 3021–3073, 2014
www.atmos-meas-tech-discuss.net/7/3021/2014/
doi:10.5194/amtd-7-3021-2014

Atmospheric Measurement Techniques Discussions
Open Access

Total column water vapour measurements from GOME-2 MetOp-A and MetOp-B

M. Grossi[1], P. Valks[1], D. Loyola[1], B. Aberle[1], S. Slijkhuis[1], T. Wagner[2], S. Beirle[2], and R. Lang[3]

[1]Institut für Methodik der Fernerkundung (IMF), Deutsches Zentrum für Luft- und Raumfahrt (DLR), Oberpfaffenhofen, Germany
[2]MPI Chemistry, Hahn-Meitner-Weg 1, 55128 Mainz, Germany
[3]EUMETSAT, Allee 1, 64295 Darmstadt, Germany

Received: 18 December 2013 – Accepted: 3 March 2014 – Published: 28 March 2014

Correspondence to: M. Grossi (margherita.grossi@dlr.de)

Published by Copernicus Publications on behalf of the European Geosciences Union.

Abstract

The knowledge of the total column water vapour (TCWV) global distribution is fundamental for climate analysis and weather monitoring. In this work, we present the retrieval algorithm used to derive the operational TCWV from the GOME-2 sensors and perform an extensive inter-comparison and validation in order to estimate their absolute accuracy and long-term stability. We use the recently reprocessed data sets retrieved by the GOME-2 instruments aboard EUMETSAT's MetOp-A and MetOp-B satellites and generated by DLR in the framework of the O3M-SAF using the GOME Data Processor (GDP) version 4.7. The retrieval algorithm is based on a classical Differential Optical Absorption Spectroscopy (DOAS) method and combines H_2O/O_2 retrieval for the computation of the trace gas vertical column density. We introduce a further enhancement in the quality of the H_2O column by optimizing the cloud screening and developing an empirical correction in order to eliminate the instrument scan angle dependencies. We evaluate the overall consistency between about 8 months measurements from the newer GOME-2 instrument on the MetOp-B platform with the GOME-2/MetOp-A data in the overlap period. Furthermore, we compare GOME-2 results with independent TCWV data from ECMWF and with SSMIS satellite measurements during the full period January 2007–August 2013 and we perform a validation against the combined SSM/I + MERIS satellite data set developed in the framework of the ESA DUE GlobVapour project. We find global mean biases as small as $\pm 0.03\,\mathrm{g\,cm^{-2}}$ between GOME-2A and all other data sets. The combined SSM/I-MERIS sample is typically drier than the GOME-2 retrievals ($-0.005\,\mathrm{g\,cm^{-2}}$), while on average GOME-2 data overestimate the SSMIS measurements by only $0.028\,\mathrm{g\,cm^{-2}}$. However, the size of some of these biases are seasonally dependent. Monthly average differences can be as large as $0.1\,\mathrm{g\,cm^{-2}}$, based on the analysis against SSMIS measurements, but are not as evident in the validation with the ECMWF and the SSM/I + MERIS data. Studying two exemplary months, we estimate regional differences and identify a very good agreement between GOME-2 total columns and all three independent data sets,

AMTD
7, 3021–3073, 2014

especially for land areas, although some discrepancies over ocean and over land areas with high humidity and a relatively large surface albedo are also present.

1 Introduction

Water vapour is a key component of the Earth atmosphere and has a strong impact on the Earth's radiative balance (Trenberth et al., 2007). It is the most potent natural greenhouse gas owing to the presence of the hydroxyl bond which strongly absorbs in the infra-red region of the light spectrum (Learner at al, 2000). As climate warms, the water vapor content in the atmosphere, which is governed by the Clausius–Claypeyron equation, is expected to rise much faster than the total precipitation amount, which is governed by the surface heat budget through evaporation (Trenberth at al., 2003). This means that there is a "positive water vapor feedback" which is expected to further amplify the original climate warming. On the other hand, the net effect of clouds on the climate is to cool the Earth surface, at least under the current global distribution of clouds, but we do not know what will be the net cooling or warming effect of clouds in a changing atmosphere. In order to study this complex interaction and evaluate climate models, observations of the effective distribution of total column water vapour (TCWV) on a global scale are fundamental.

The water vapour distribution plays a major role for both meteorological phenomena and climate via its influence on the formation of clouds and precipitation, the growth of aerosols and it is a driving parameter in the reactive chemistry related to ozone and the hydroxyl radical. Hence, advancing in understanding of variability and change in water vapor is vital, especially considering that, in contrast to most other greenhouse gases, the H_2O distribution is highly variable. However, for a long time the important role of water vapour did not originate an adequate experimental activity. Only in 1993, it was included in the list of greenhouse gases by the World Meteorological Organisation (WMO) and difficulties in observing the water vapour in the troposphere have long hampered observations and modeling studies. Starting from the 1990s, accurate

AMTD
7, 3021–3073, 2014

measurement techniques have been developed and, today, a large variety of in-situ and remote sensing techniques for the measurement of integrated water vapour can be operated from different platforms. Nonetheless, significant limitations still remain in coverage and reliability of observations humidity data sets. The traditional humidity profiling with ground-based radiosonde can provide water vapour profiles with good resolution over all weather conditions, but they are usually available only twice a day, at sparse locations over the globe (mostly industrialized areas and land surfaces), and they often contain systematic biases (Wang et al., 2002) and spurious changes (Gaffen et al., 1991). Since 1994, when the Global Positioning System (GPS) became full operational, considerable efforts have been put to develop and improve methods to derive atmospheric water vapour using ground-based GPS measurements (e.g., Bevis et al., 1992, 1994; Rocken et al., 1993, 1997, 2000) at very high temporal resolution (about 30 min). However, only satellite observations offers the unique opportunity to study the spatial and temporal variability of water vapour on a global scale.

Complementary to ground-based measurements, which provide accurate information on the H_2O concentration, satellite observations allow us to assess the distribution of the column-integrated (the so-called total column) water vapour also in remote places with none or only few in-situ measurements, but they are typically limited in their vertical and temporal resolution. Most commonly used for the retrieval of water vapour from space are microwave sensors, like the Special Sensor Microwave Imager (SSM/I), which are able to provide measurements at high spatial (horizontal) resolution (Bauer and Schluessel, 1993), but are usually constrained on ice free ocean areas. Data from these instruments are operationally assimilated in numerical weather prediction reanalysis models like the ERA Interim from the European Centre for Medium Range Forecasts (ECMWF, Dee et al., 2011a, b) and, until the beginning of this century, represented the only consistent long timescales data set for water vapour. Sensors operating in the near infrared, like the Medium Range Resolution Imager Spectrometer (MERIS) on ENVISAT (Li et al., 2006), can derive water vapour also over land. Unfortunately, NIR instruments cannot see through clouds, but are limited to sun-glint

AMTD
7, 3021–3073, 2014

or above-cloud conditions over ocean, because of the very low albedo of the ocean-surface in the NIR, which also limits the retrieval. A recently developed method for the retrieval of water vapour distribution is the utilization of data from the GPS satellites (see e.g. Dai et al., 2002). Despite the relative small amount of data, GPS measurements from space and ground are valuable because their information complement the one provided by satellite radiance measurements.

Sensors covering the UV and visible range with a relative high spectral resolution like the Global Ozone Monitoring Experiment (GOME) on ERS-2 (Burrows et al., 1999), can accurately map the column densities of the atmospheric H_2O over all surfaces. The analysis is performed in the visible spectral range, thus it is very sensitive to the H_2O layers close to the surface, but, similar to MERIS, the retrievals are typically hampered by clouds. GOME data have been used, among others, for the study of long term variations in tropospheric water vapor trends (Mieruch et al., 2008; Wagner et al., 2006) and to monitor and investigate inter annual climate variability phenomena observed on Earth, like El Niño/La Niña (Wagner et al., 2005; Loyola et al., 2006). A second generation of this kind of instruments was represented by the Scanning Imaging Absorption Spectrometer for Atmospheric Chartography (SCIAMACHY, Bovensmann et al., 1999) on the ENVISAT platform. Current UVN sensors are the GOME-2 instruments, the subject of the current study, on board of the MetOp-A and MetOp-B satellites. The GOME-2 spectrometers, which observe about four to eight times smaller ground pixels then its predecessor GOME, lay the foundation for a consistent data record of H_2O GOME-type observations, which spans more than 18 years already and will be further extended by GOME-2/MetOp-C, a third satellite which is planned to be launched in 2018.

Total Column Water Vapour (TCWV) from measurements of the GOME-2 instruments aboard EUMETSAT's MetOp-A and MetOp-B satellites has already proved to be a valuable input quantity in climate monitoring (Noel et al., 2008; Slijkhuis et al., 2009; Kalakoski et al., 2011; Mieruch et al., 2010), and could be useful for numerical weather predictions. In contrast to other satellite data sets, the GOME-2 product has the advantage that it covers the entire Earth, including both ocean and continents,

AMTD
7, 3021–3073, 2014

leading to a more consistent picture of the global distribution of the atmospheric humidity. Long-term satellite data sets are essential for atmospheric monitoring and the impact of human intervention in a changing environment has brought about increasing concern for detecting trends in water vapour. Recently, the ESA DUE Glob Vapour project (Schröder et al., 2012a) has focused on the development of multi-annual global water-vapour data sets and, among other deliverable, has provided a first version of a consistent TCWV data set from the GOME, SCIAMACHY and GOME-2 sensors for the time period 1996–2008. In the framework of the Glob Vapour project, extensive validation activities were carried out, but the results pointed out large differences with positive and negative bias values on regional scales (Schröder and Schneider, 2012).

In this paper, we present the H_2O retrieval algorithm used for the operational EUMETSAT's Satellite Application Facility on Ozone and Atmospheric Chemistry Monitoring (O3M-SAF) water vapour products from GOME-2 and the validation against independent satellite instruments and model data. On the basis of this validation, we are able to estimate the accuracy of the retrieval algorithm and we can make a sound assessment of the quality and consistency of GOME-2 TCWV product.

After a short description of the GOME-2 type instruments in the following, Sect. 3 gives a detailed overview of the H_2O retrieval algorithm and introduces the total column water vapour data used for the validation with model data and independent satellite measurements. In Sect. 4 the GOME-2 water vapour columns are compared during their overlapping time frame January 2013 through August 2013. We perform a quantitative analysis of the distribution of daily and monthly mean biases. The results of the GOME-2 TCWV validation with ECMWF data and satellites measurements from SSMIS, SSM/I and MERIS for the full period 2007–2012 is illustrated in Sect. 5. Finally, conclusions are drawn in Sect. 6.

AMTD
7, 3021–3073, 2014

2 GOME-2 instruments

The GOME-2 sensor (Callies et al., 2000) is the follow up of the Global Monitoring Experiment (GOME) launched in 1995 on ERS-2 (Burrows at al., 1999), and the SCIAMACHY sensor launched 1995 on ENVISAT (Bovensmann et al., 1999). GOME-2 is a nadir viewing scanning spectrometer which covers the same spectral range as GOME, i.e., from 240 to 790 nm, with spectral resolution of about 0.54 nm in the visible spectral region. Additionally, two polarization components are measured with polarization measurements devices (PMDs) at 30 broad-band channels covering the full spectral range at higher spatial resolution. The German Aerospace Centre (DLR) plays a major role in the design, implementation and operation of the GOME-2 ground segment for trace gas products, including total column water vapour, as well as cloud properties in the framework of the EUMETSAT O3M-SAF project.

GOME-2 is an improved version of the GOME instrument on the ERS-2 satellite (Munro et al., 2006), but we can identify important differences between them. First, the spatial resolution of the GOME data is 320 km × 40 km, whereas the GOME-2 instruments have a smaller nominal ground pixel size (typically 80 km × 40 km). Because of the improved spatial resolution, GOME-2 data are less influenced by partly cloudy scenes and the intruments are also able to detect strong spatial gradients in the H_2O distribution. Second, the default swath width of the GOME-2 scan is 1920 km, while both GOME and SCIAMACHY have a scan width of 960 km. Finally, the GOME-2 instruments employ only about 1.5 day to reach global coverage at the equator, while GOME/ERS-2 requires about three days[1].

In Table 1 we summarize the characteristics of different GOME-type sensors.

The first GOME-2 instrument was mounted on the MetOp-A satellite, which follows a Sun-synchronous orbit with a mean altitude of 817 km. The overpass local time at the equator is 09:30 LT with a repeat cycle of 29 days. MetOp-A was launched on

[1] After the failure of the ERS-2 tape recorder in June 2003, GOME measurements have been limited to the Northern Hemisphere and the Antarctic.

AMTD
7, 3021–3073, 2014

19 October 2006 and GOME-2 TCWV products are available from January 2007 onwards. A second GOME-2 type sensor, on board of the MetOp-B satellite was launched on the 17 September 2012 and is fully operational since December 2012. At the 15 of July 2013 GOME-2/MetOp-A started to operate in tandem with GOME-2B on a reduced swath width of 960 km and with an increased spatial resolution (40 by 40 km), while GOME-2/MetOp-B continued to operate in 1920 km swath mode and without interruption by a monthly "narrow-swath" day. This configuration allows the use of the higher spatial resolution data to further improves the consistency of the two products in the overlap regions of the GOME-2A and GOME-2B orbits.

The third and final satellite of the EUMETSAT Polar System series, GOME-2/MetOp-C, is planned to be launched in 2018, and it is foreseen to guarantee the continuous delivery of high-quality H_2O data until 2023.

3 GDP 4.7 H_2O column algorithm

In the framework of the EUMETSAT O3M-SAF project, the algorithm used to generate the operational H_2O product is the level-1-to-2 GOME Data Processor (GDP) version 4.7, integrated into the Universal Processor for Atmospheric Spectrometers (UPAS, version 1.3.9) processing system at DLR.

A variety of methods for the retrieval of the Total Column Water Vapour (TCWV) from space-born spectrometers operating in the visible region has been developed (AMC-DOAS: Noël et al., 1999; Lichtenberg et al., 2010; ERA: Casadio et al., 2000; OCM: Maurellis et al., 2000; IGAM: Lang et al., 2003, 2007; Classical DOAS: Wagner et al., 2003). In contrast to most other methods, the GDP 4.7 algorithm for the retrieval of water vapour is directly based on a classical Differential Optical Absorption Spectroscopy (DOAS, Platt, 1994) performed in the wavelength interval 614–683 nm and does not include explicit numerical modeling of the atmospheric radiative transfer. One specific advantage of the DOAS method is that it is only sensitive to differential

AMTD
7, 3021–3073, 2014

absorptions, which makes the retrievals less sensitive to instrument changes or instrument degradation.

The algorithm consists of three basic steps (described in detail by Wagner et al., 2003, 2006): (1) DOAS fitting, (2) non-linearity absorption correction and (3) Vertical Column Density (VCD) calculation.

In the first step, the spectral DOAS fitting is carried out, taking into account the cross sections of O_2 and O_4, in addition to that of water vapour. A single H_2O cross section is used, based on line-by line computations using HITRAN (Rothman et al., 2009) H_2O line parameter at 290K, followed by a GOME-2 slit function convolution. To improve the broadband filtering, 3 types of vegetation spectra are included in the fit. They are included also over water, as marine chlorophyl-containing substances may show similar spectra and can cause strong interference with atmospheric absorbers (Wagner et al., 2007). In addition, we use a synthetic Ring spectrum calculated from the sun spectrum (Gomer et al., 1993; Wagner et al., 2009) to correct for the Ring effect (filling-in of well-modulated solar and absorption features in the Earth shine spectra) and, finally, an inverse solar spectrum to compensate for possible offsets, e.g. caused by instrumental stray light.

Since the highly fine structured H_2O (and O_2) absorption bands cannot be spectroscopically resolved by the GOME instrument, the water vapour slant column density (SCD: the concentration integrated along the light path) is no more a linear function of the atmospheric H_2O column density (Solomon et al., 1989; Wagner et al., 2000). In the second step of our retrieval, we apply a correction for the absorption non-linearity effect. The corrections factors are calculated from numerical simulations of this effect by mathematical convolution of the high resolved H_2O spectrum with the instrument slit function (Van Roozendael et al., 1999; Wagner et al., 2003) and they are larger for higher H_2O SCDs. For example, for an atmospheric H_2O SCDs of 1.5×10^{23} mol cm^{-2} (~ 4.5 g cm^{-2}) the underestimation is about 30 %.

In the last step, the corrected water vapour slant columns determined with the DOAS fitting are converted to geometry-independent Vertical Column Densities (VCDs)

AMTD
7, 3021–3073, 2014

through division by an appropriate Air Mass Factor (AMF), which in this case is derived from the measured O_2 absorption. We divide the H_2O SCD by a "measured" AMF which is defined as the ratio between the simultaneously retrieved SCD of O_2 and the known VCD of O_2 for a standard atmosphere. The desired total column water vapour is computed as follows:

$$\Omega_{H_2O,0} = \frac{\Omega_{H_2O,\theta}}{A_{O_2}} = \frac{\Omega_{H_2O,\theta}}{\Omega_{O_2,\theta}/\Omega_{O_2,0}}, \quad (1)$$

where $\Omega_{x,0}$ is the VCD, $\Omega_{x,\theta}$ is the SCD and A_x is the AMF of the chemical species x. This simple approach has the advantage that it corrects in first order for the effect of varying albedo, aerosol load and cloud cover using the satellite observations themselves, without additional independent information which is usually also not available. However, the underlying assumption that the AMF of O_2 is similar to the AMF for water vapour can produce systematic differences in the retrieval. Because the vertical profile of H_2O is much more peaked in the troposphere with respect to that of O_2 (the H_2O scale height is only about 2 km compared to 8 km for O_2), the measured AMF derived from the O_2 absorption is in general larger than the AMF for water vapour. In the case of low lying clouds, for example, the dominant part of H_2O column is located near the surface and therefore shielded, while most of the O_2 contribution is still above the clouds.

All in all, the errors in the individual H_2O VCD measurements can be quite large due to the application of an O_2 AMF. One possibility to correct these errors would be to use the appropriate AMFs derived from radiative transfer (RT) calculations instead. In the future, we plan to identify, and possibly correct, the influence of clouds and surface albedo on the TCWV using the LIDORT RT model (Spurr, 2008). However, such calculations are complicated because typically the atmospheric aerosol extinction profile is not known, and clouds strongly affect RT calculations. Because of these difficulties, we follow a different approach here: we simply introduce a correction factor look-up table

AMTD
7, 3021–3073, 2014

in the AMF computation:

$$\Omega_{H_2O,0} = \frac{\Omega_{H_2O,\theta}}{A_{O_2}} \times C_{ratio} = \frac{\Omega_{H_2O,\theta}}{\Omega_{O_2,\theta}/\Omega_{O_2,0}} \times C_{ratio}. \quad (2)$$

The factor C_{ratio} depends on the solar zenith angle (SZA), on the line of sight angle (LOS) and relative azimuth (RAZ) of the satellite instrument and on the surface albedo (Alb). Moreover, the exact vertical profile of H_2O in the troposphere and the cloud cover have a strong impact. The correction factors were derived from radiative transfer calculations using the Monte Carlo Atmospheric Radiative Transfer Inversion Model (McArtim, Deutschmann et al., 2011) and taking into account an average H_2O profile calculated from relative humidity profiles assuming an average lapse rate (Minschwaner and Dessler, 2004; Wagner et al., 2006) and an O_2 profile from the US standard atmosphere. The relative sensitivity of the measured O_2 absorption compared to H_2O absorption also varies significantly depending on surface albedo values. In the RTM the correction factor was computed depending on surface albedo (and cloud fraction). We used the albedo database derived from GOME observations (Koelemeijer et al., 2003) for high latitude ($> 50^\circ$) and from SCIAMACHY observations (Grzegorski, 2009) at mid and low latitudes ($> 40^\circ$) in order to derive the dependency of the computed AMFs to the actual surface albedo. It should be mentioned that the global surface albedo map described above is the only external information needed in the retrieval algorithm (in addition to the average H_2O and O_2 profiles), and therefore this GOME-2 H_2O VCD product is especially valuable for long-term series and climatological studies.

3.1 Error budget and cloud masking

The error budget in the H_2O data product can be separated in two parts: errors affecting the retrieval of the slant columns (DOAS-related errors), and errors affecting the conversion of the SCD into VCD (AMF-related errors). However, this last errors are difficult to quantify, because the water vapour AMF is not based on explicit RT calculations, and there may be also compensating effects. For example, in the case of snow

AMTD
7, 3021–3073, 2014

surfaces, the high surface reflectivity would lead to a relatively high sensitivity for H_2O in the lower troposphere, and hence a lower AMF-ratio of O_2 to H_2O, but above cold surfaces the tropospheric H_2O column is reduced, causing the opposite effect. Here we take into account the following potential error sources: relative fit error of H_2O and O_2, uncertainties in the spectroscopic data (about 10 %) and especially uncertainties due to clouds. The total, relative error can be derived by the following formula:

$$\Delta_{\text{total}} = \sqrt{\Delta^2_{H_2O} + \Delta^2_{O_2} + (0.1)^2 + \Delta^2_{\text{RTM}}}. \quad (3)$$

The source of error due to clouds (Δ^2_{RTM}) increases with decreasing O_2 SCD, indicating strong cloud shielding. On the GOME-2 H_2O product, therefore, cloudy conditions are flagged.

In order to remove potential systematic cloud effects which might still appear in the water vapor product due to the different altitude profile of H_2O and O_2, in our latest version of the retrieval algorithm (GDP 4.7) we use two cloud indicators to identify and flag cloudy pixels. The first cloud flag is set if the product of cloud fraction and cloud top albedo exceeds 0.6 (anomalously high cloud top reflection). In this case also the H_2O total column is set to "invalid" as the pixel might be considered fully clouded. The GOME-2 cloud fraction is determined with the OCRA algorithm using broadband radiance measurements in the UV/VIS range, while cloud-top height and cloud-top albedo are retrieved with the ROCINN algorithm using the spectral information in the Oxygen-A band in and around 760 nm (Loyola et al., 2007 and 2010). The GOME-2 detector read-out timing may induce spatial aliasing effects for highly variable scenes in the case that the retrievals use measurements from largely separated detector channel. The PMD measurements are aligned to the O2 A-band measurements (end of channel 4) to avoid spatial aliasing effects between the OCRA/ROCINN derived cloud properties. Possible spatial aliasing effects between the cloud properties and the water vapour measurements (begin of channel 4) are minimized by using a rather conservative cloud screening scheme.

AMTD
7, 3021–3073, 2014

The second H_2O cloud flag is set if the retrieved O_2 slant column is below 80 % of the maximum O_2 SCD for the respective solar zenith angle (roughly when about 20 % from the column to ground is missing). Especially for low and medium high clouds, the relative fraction of the VCD from the ground which is shielded by clouds for O_2 and H_2O can be quite different. Therefore, we require that the main part of the O_2 column is present. The maximum values of the O_2 SCD have been derived from measured optical depth of the O_2 absorption along GOME satellite orbits as a function of the solar zenith angles and implemented in a look-up table in the retrieval code. We also consider the line of sight dependence of the O_2 threshold for mainly cloud-free observations by multiplication for an additional function (Wagner et al., 2011). The choice of having a threshold of 80 % of the maximum values represents a good compromise with respect to the number of measurements still available after selection and the correction of the strongest cloud effects on the total column water vapour product. This second cloud flag also rejects observations with high surface elevation, e.g. the Himalayas or the Andes.

3.2 Scan angle dependency correction

As already mentioned, the GOME-2 observations have a much wider swath compared to GOME and SCIAMACHY (see Table 1). While this broader swath results in a largely improved coverage, also some modification to the H_2O retrieval becomes necessary. In particular, we observe that the water vapour columns present a significant Scan Angle Dependency (SAD) which strongly affects the quality of the product. This scan angle dependency of the GOME-2 H_2O columns is very similar for MetOp-A and MetOp-B.

There is a bias up to 1 g cm^{-2} between the H_2O product for the west and east part of the swath and the central ground pixels. The effect is particularly strong over ocean areas, while the land surface is less affected. There are two major contributing factors. First, the accuracy of the retrieved water vapour columns is reduced because of sun-glint over ocean regions which may strongly enhance the backscattered radiation, especially at low wind speed (highly specular reflection). In this case, the observations

AMTD
7, 3021–3073, 2014

are contaminated by the bright pattern of the specular reflection of the sun by the wavy sea surface. The GOME-2 algorithm can distinguish sun-glint areas by analyzing the broadband polarization measurements (Loyola et al., 2011), but the pixels we select with this method (typically less than 4 % of the total) represent only few measurements in extreme sun-glint geometry. Therefore, we still require a rigorous correction for the small signal of water-leaving radiances in directions away from the glitter. Second, the accuracy of the surface albedo data available for the oceans is limited, and therefore a constant albedo (0.03) is used in the AMF calculation for the sea surface (Grzegorski et al., 2004).

An accurate analysis of the GOME-2 H_2O columns retrieved with a previous version of the GDP algorithm (GDP 4.6) revealed a systematic SAD already in the H_2O SCD, especially for cloud-free pixels, which suggested a correlation between a simplified Lambertian assumption used to describe the Earth reflectivity and the SAD. From radiative transfer calculations using Bidirectional Reflectance Distribution Function (BRDF) kernels based on a Cox–Munk distribution (Cox and Munk, 1954), we found that using a simple Lambertian approach and ignoring the BRDF, we underestimate the AMF over ocean in the East regions of the scan (and overestimate it in the West regions) up to 30 % (Valks et al., 2012). Some residual line of sight dependence is likely due to the Rayleigh single scattering contribution, since the instrument is polarization sensitive. Moreover, as mentioned in Sect. 3, in order to compute the H_2O VCD we use the simultaneously observed O_2 slant column density and we introduce a correction factor which accounts for the different altitude profile of H_2O and O_2. Since the look up tables containing the correction factors are computed for average conditions of cloud cover, albedo, and a single H_2O profile, some residual SAD might remain especially in more extreme atmospheric scenarios.

In GDP 4.7 we introduce an empirical statistical correction for the scan angle dependency, based on the full 6 years time-series of GOME-2/MetOp-A measurements (2007–2012). Multi-annual monthly mean H_2O total columns are created and employed to select the latitudinal binned regions which contains a sufficient large number of

AMTD
7, 3021–3073, 2014

measurements (we require that the number of measurements for the different scan angles at a given latitude does not vary by more than 20 %). In this way we avoid that the correction is affected by natural variability in the H_2O columns. We use scan angle read-outs toward the middle ground pixel as reference values to normalize the H_2O total column for every forward angle position and derive a self-consistent correction. Finally, we fit a polynomial to the normalized measurements in order to remove outliers and obtain a smooth correction function. Outside the valid latitudinal range we interpolate between the last valid value and 1 (i.e. no correction) for ±90° latitude. A similar algorithm was originally developed for correcting the scan-angle dependency of GOME-2 total ozone product (Loyola et al., 2011).

We implemented two different corrections over land and over sea, to take into account the diverse reflectivity properties of the surface and we found that the bias between East and West pixels depends on the viewing geometry; i.e. the correction values are a function of scattering angle, latitude and vary from month to month. In the left panel of Fig. 1, we can see the SAD correction for land, while in the right panel the correction applied over ocean regions is shown. In both figures we can distinguish the water vapour VCD before (solid line) and after (dashed line) the empirical correction for the scan angle dependency. The lines refer to latitudinal averaged quantities in the northern, tropical and Southern Hemisphere regions for January 2013. While in austral summer (December–February) the correction is larger in the 20–50° south regions, in the Northern Hemisphere summer months (June–August) it is larger for the 20–50° north region.

Figure 2 shows the global distribution of the H_2O VCD derived from GOME-2B measurements for the 7 January 2013 with (left panel) and without (right panel) SAD correction for cloud-screened measurements only. The white regions in the map show the areas where the product of cloud fraction and cloud top albedo exceeds 0.6, while the O_2 cloud screening rejects mostly GOME-2 measurements over the west part of scan, since these are measurements with small AMF and low GOME-2 sensitivity for H_2O. The net effect of the empirical correction is to reduce the bias in the water vapour

AMTD
7, 3021–3073, 2014

column density distribution between the east and west part of the GOME-2 orbit. Comparing the left and right panel of Fig. 2 we can see differences especially in the equatorial region, where the H_2O total column presents lower values in the east part of the scan when applying the SAD correction (e.g. over the Pacific Ocean near the Mexican coast).

GOME-2 Level 2 TCWV and cloud products generated using the GDP 4.7 algorithm are available from the DLR ftp server in HDF5 format. Information about the operational offline water vapour product can be found at http://atmos.caf.dlr.de/gome2. In the same website are also available documents, reports, as well as quick look maps and links to related information.

4 GOME-2A vs. GOME-2B

We compare the GOME-2/MetOp-B H_2O VCDs with those from its predecessors GOME-2/MetOp-A. This initial study is based on more than eight months of overlap between the two satellites from December 2012 to August 2013. We perform the intercomparison between GOME-2A and GOME-2B data taking into account either (mostly) cloud-free or all available measurement for one particular day and monthly means. For the monthly comparison, we first analyze the bias between the monthly mean distribution of GOME-2A and GOME-2B water vapour columns, and then, in order to make the data selection in the two instruments as similar as possible, we have also performed the comparison using only co-located measurements. A quantitative analysis of the bias between GOME-2A and GOME-2B as a function of the latitude concludes this section.

4.1 Daily GOME-2 comparison

In the top panels of Fig. 3 we show a map of the H_2O columns for the 7 January 2013 from GOME-2A (left panel) and GOME-2B (right panel) measurements and provides

AMTD
7, 3021–3073, 2014

a first illustration of the geophysical consistency of the total H_2O column products from the different instruments. In both cases we applied consistently a SAD correction over ocean and land areas. Overall, we observe a very good agreement between the two data sets and the same spatial patterns in the humidity distribution, with high values in the tropics and low humidity at higher latitudes. Since the GOME-2 products are only derived from daylight observations, a large area around the Arctic is blanked out in the Northern Hemispheric winter. Here, we do not apply any cloud mask to the data to show the daily coverage of the two GOME-2 instruments.

In the bottom panels of Fig. 3 we investigate the differences between GOME-2A and GOME-2B water vapour column for the 7 January 2013 when the SAD correction is applied to the two data sets (right panel) and without SAD correction (left panel). The inter-comparison has been performed using cloud-free and co-located pixels. Co-location areas are determined applying the following criteria: 55 km for the maximum distance between 2 measurements in the chosen day. In the tropics the number of measurements is drastically reduced not just because of the larger chance of clouds, but principally because we have the smallest overlap between the GOME-2A and GOME-2B orbits. On average, the H_2O VCD for GOME-2B is slightly higher than for GOME-2A product, independently on the presence of a SAD correction in the two data sets (i.e. if we use GDP 4.6 or GDP 4.7 retrieval) with mean bias values of $-0.05\,\mathrm{g\,cm^{-2}}$. The GOME-2A and GOME-2B co-planar orbits are 174° out of phase. This results in a temporal separation of the measurements at the co-locations of approximately 48 min and leads to differences in the water vapour total column because of tropospheric dynamics. The overall mean bias and the Root Mean Square Error (RMSE) values do not change significantly using the GOME-2 data with and without the SAD correction. However, because of the additional scan-angle bias, at single locations the difference between GOME-2A and GOME-2B water vapour is larger without SAD correction, as we can see comparing the left and right plot of Fig. 3. This is due to the fact that when we are looking at the daily co-locations we are comparing data from different parts of GOME-2A and GOME-2B swaths (and thus different lines of sight). Using the data sets

AMTD
7, 3021–3073, 2014

without SAD correction (left panel of Fig. 3) we can see that the differences are alternating between positive and negative values, depending on whether we are collocating the East part of the GOME-2A swath with the West part of the GOME-2B swath or vice versa. This effect is reduced in the GDP 4.7 data sets (right panel of Fig. 3). We can observe now null bias (in green) in extended sub-tropical regions, like continental Northern Africa and Asia. Remaining differences in the tropics are mainly related to the presence of low clouds, the asymmetric cloud screening and low statistics.

4.2 Monthly GOME-2 comparison

The global average monthly mean bias between GOME-2A and GOME-2B data sets for the period January 2013 to August 2013 is shown in Fig. 4. From the 15 July to the end of August GOME-2A operates in tandem mode, and the overlapping area between the orbits of the two satellites is reduced. However, the mean bias values are consistent with the one retrieved in previous months. Averaging over the full time period, we find a small mean negative bias of $-0.012 \pm 0.016\,\mathrm{g\,cm^{-2}}$, while the biggest discrepancies are observed in January 2013 (mean bias of $-0.025\,\mathrm{g\,cm^{-2}}$). GOME-2B tends to produce slightly larger H_2O total column values than GOME-2A, but not more than 1.25 %. Studying the spatial distribution of the bias in January 2013, we observe that less than 3 % of the locations present a bias bigger than $0.5\,\mathrm{g\,cm^{-2}}$ in absolute value. The mean difference between GOME-2A and GOME-2B H_2O VCDs is still within the optimal accuracy threshold defined by the Product Requirements Document (PRD; Hovila er al., 2008). This shows that the GOME-2B H_2O total column product can be used for scientific purposes to extend the GOME-type H_2O time series.

To access the consistency between the two samples, we performed an orthogonal regression using the gridded monthly mean data. The grid cells used to bin the GOME-2 measurements have an extent of 0.5° latitude ×0.5° longitude. Figure 5 shows the scatter plot of cloud-screened GOME-2A data against GOME-2B for January 2013 together with the histogram of the distribution of the differences GOME-2A – GOME-2B.

AMTD
7, 3021–3073, 2014

The slope of the regression is very close to unity (0.992) and the offset is very small and negative ($-0.009\,g\,cm^{-2}$), consistently with the mean bias results.

To investigate the differences between the GOME-2A and GOME-2B water vapour column as a function of latitude, we have repeated the validation exercise for co-located (within 24 hours) measurements, with and without cloud mask, and we further computed the zonal averages for 2.5° latitude intervals. Figure 6 shows the comparison of zonal total column water vapour values for January 2013 in two different cases: for (mostly) cloud free measurements (left panel) and for all measurements (right panel). The points in the left panels of each plot represent the individual mean water vapour measurements as a function of latitude (red for GOME-2A, green for GOME-2B). From this plots we can infer that there is an excellent agreement between GOME-2A and GOME-2B measurements for all latitudes. In order to examine more clearly the latitudinal variations, in the right panels of each plot (Fig. 6), we show the difference GOME-2B – GOME-2A H_2O total column. The largest deviations occur at low latitudes (about ±10°). On average, at these locations the GOME-2B total columns are slightly larger than the GOME-2A columns (about 2–3 % larger in relative value), as inferred also from the scatter plots (Fig. 5). The fractional difference is always positive, especially in the tropical area, which means that the GOME-2B data present a small wet bias with respect to GOME-2A. The maximum bias reaches $0.117\,g\,cm^{-2}$ (2.7 %), and the mean bias is higher in the Southern Hemisphere than in the northern one. We can also notice that the extent of the scatter is generally bigger for cloud-free measurements than for unfiltered data because the smaller number of data points due to the cloud selections translates in a larger RMSE in the former case (see Grossi et al., 2013).

5 Validation results and discussion

To have a sound assessment of the quality of the satellite products, we performed an extensive validation of both the GOME-2A and the GOME-2B products. We compared the GOME-2 H_2O total column product to 3 different data sets. Each of these data sets

AMTD
7, 3021–3073, 2014

has his own advantages and disadvantages and therefore, from the different comparisons, we can study different properties of the GOME-2 data sets.

First, GOME-2 results are compared with corresponding model data from the European Centre for Medium Range Weather Forecasts (ECMWF). We use the ERA interim reanalysis data (Dee et al., 2011a, b) at all available time steps.

The second data set is based on passive microwave observations from SSMIS orbits of the F16 satellite. These data are produced by Remote Sensing System and sponsored by the NASA earth science MEaSUREs DISCOVER projects (REMSS, http://www.ssmi.com/ssmi). They are available over ocean only and rely on independent calibration against radiosonde data (Wentz, 2013). However, they include also the TCWV for cloudy scenes, both day and night overpasses and span a very large time range (SSM/I has been in orbit since 1987).

The third sample we used relies on the Glob Vapour combined SSM/I + MERIS TCWV Level 3 data set (Schröder et al., 2012b) derived within the ESA DUE Glob Vapour project. Both data sets were processed independently and combined afterward to fit in one file per day and month, respectively. The combined data set is based on TCWV retrievals from measurements in the microwave range taken by SSM/I over ocean (F13 and F14 satellites) and measurements of the visible and near infrared by MERIS (over land and coastal regions). In particular, MERIS provides water vapour column amounts for cloud free scenes for day time overpasses over land with a very good spatial resolution. Like for GOME-2, the quality of the retrievals is mainly determined by uncertainties in clouds detection.

All validations are performed for GOME-2 H_2O total columns which are not flagged as cloud-contaminated on the data product. The "H_2O flag" is set when the measured surface reflection indicates sever cloud cover (cloud albedo × cloud fraction > 0.6) or when the O_2 absorption is too low. The current limit requires that at least 80 % of the O_2 column must be present (see Sect. 3.1).

In Fig. 7 (top panel) we show a time series of globally averaged total bias based on daily and monthly means of the TCWV distribution between GOME-2A and the 3

AMTD
7, 3021–3073, 2014

different data sets described above and for the time period January 2007–August 2013. For the last part of 2013 we have computed also the bias between the most recent GOME-2B results and the ECMWF and SSMIS retrievals. The agreements between GOME-2 data and the independent measurements we consider is very good for all comparisons: the mean bias for the full time series is very close to 0, while the Root Mean Square Error (RMSE) varies between 0.4 and 0.7 $g\,cm^{-2}$ (see Table 2). Since the GOME-2B total column data are typically larger than the GOME-2A data (see Sect. 4), also the bias is shifted towards higher values in this case. The validation has been performed in such a way that positive and negative bias imply respectively larger and lower GOME-2 data. In the bottom panel of Fig. 7 we also report the monthly averaged TCWV values for the GOME-2A and GOME-2B measurements in order to assist the interpretation of the bias results. The time series are computed for the ocean data-set only and for all surfaces. We can notice that the H_2O VCD products exhibit a minimum during the northern hemispheric winter and a maximum in the summer months and that the TCWV values are typically larger over ocean surfaces.

As an exemplary time series, we can analyze the inter-comparison between GOME-2A and SSMIS data, the magenta line and points in the top panel of Fig. 7. More than six years overlap between GOME-2A and SSMIS data provides a very good opportunity to investigate the seasonal dependence of the results. In this case, we observe a bias, which is high in NH summer and low in NH winter, with the averaged TCWV for SSMIS being slightly higher than GOME-2 (0.028 $g\,cm^{-2}$, see Table 2). The monthly averaged bias ranges from $-0.067\,g\,cm^{-2}$ in January 2010 and January 2007 to 0.13 in July 2013. We can indeed infer a seasonal cycle of the geographic distribution of the bias between clouds corrected scenes (GOME-2) and all conditions (in this case SSMIS) data sets, which is probably caused, among other reasons, to the seasonality of cloud properties in same locations, as well as the variability of geographic distribution of major cloud structures as the Intertropical Convergence Zone (ITCZ), but is less pronounced in n the SSM/I + MERIS and ECMWF comparisons.

AMTD
7, 3021–3073, 2014

For the SSM/I + MERIS data set (in green), we can see that the seasonal behavior is not as evident as for SSMIS, as a result of the different biases over land (MERIS) and sea (SSM/I). In general the MERIS measurements present a wet bias with respect to all other data sets, which might be partly caused by spectroscopic uncertainties, such as the description of the WV continuum (Lindstrot at al., 2012). Interpreting these results, we should also have in mind the limitations of the GOME-2 retrieval. Although, as discussed before, a specific advantage of the visible spectral region is that it is sensitive to the water vapour concentration close to the surface and that it has almost the same sensitivity over land and ocean, the accuracy of an individual observation is reduced for cloudy sky observations. In addition, the GOME-2 observations, which are made at 09:30 LT, cannot be representative of the daily, and therefore monthly, average H_2O values in regions with a pronounced WV diurnal cycle.

Finally, the ECMWF data show very smallest oscillation around the mean bias against GOME-2A measurements. The global mean bias is slightly positive ($0.03\,g\,cm^{-2}$), but we can observe the compensating effect of having land and sea retrievals (the amplitude of the winter–summer oscillation is $0.07\,g\,cm^{-2}$ at most). As for the SSMIS validation, also in this case we studied daily collocations, in order to derive conservative estimates for the precision of our water vapour retrieval. This is important to remove at least part of the bias introduced by the presence of cloudy regions in microwave measurements and simulated data.

In order to interpret these results and to assess the observed biases and seasonal cycle, in the following sections we further discuss the validation method we use and show the global distribution of the bias between GOME-2A and the 3 independent data sets for two exemplary months (February and August 2008).

5.1 Comparison with ECMWF TCWV model data

GOME-2A and GOME-2B measurements are compared to model simulations of the European Centre for Medium Range Weather Forecasts (ECMWF). The H_2O total column simulation data used here are based on the total water vapour output of the

AMTD
7, 3021–3073, 2014

ERA-Interim reanalysis data set (Dee et al., 2011a, b). ERA-Interim is the latest global atmospheric reanalysis produced by the ECMWF and provides a coherent record of the global atmospheric evolution constrained by the observations during the period of the reanalysis (1979 to present). An advantage of using reanalysis data for validation assessment is that they provide a global view that encompasses essential climate variables in a physically consistent framework. The results are produced with a sequential data assimilation scheme, in which available observations are combined with prior information from forecast models to estimate the evolving state of atmospheric water vapour. The accuracy of the data assimilation scheme, however, will depend on the quality and availability of observations in the selected time frame.

In this study, we use ECMWF model outputs between January 2007 and August 2013 and we combine the ERA Interim forecast 12 h values to derive a daily mean H_2O vertical column. For the inter comparison, we first determine co-locations of daily gridded water vapour from GOME-2 and ECMWF data on a regular $1.5^\circ \times 1.5^\circ$ spatial grid, and then calculate daily and monthly mean differences (GOME-2 – ECMWF).

In the top plots of Fig. 8 we can see the monthly mean TCWV product in February 2008 obtained from daily collocation of ECMWF and GOME-2A data. We choose this month as representative of the water vapour distribution in the NH winter season. In the bottom plots of Fig. 8 one can see the corresponding ECMWF and GOME-2A measurements in August 2008. We can observe in all panels a high humidity in the tropics and low humidity at higher latitudes. Also the movement of the inner tropical convergence zone with seasons is clearly visible from the shift of the high water vapour column in the tropics between February and August 2008. In both hemispheres, the total column precipitable water vapour distribution follows the seasonal cycle of the near surface temperature: the tropical total column H_2O has a maximum during the Northern Hemisphere (NH) summer, and a minimum in winter. Looking at the differences between GOME-2A and ECMWF monthly means, we can distinguish only few regions with obvious discrepancies, like in the Amazonian and central Africa in February, or the south-east Asia in August 2008. Overall, we find similar spatial patterns in the H_2O

AMTD
7, 3021–3073, 2014

distribution in the ECMWF and GOME-2A data sets. From these results we can therefore already confirm that the GOME-2 retrievals can achieve a good accuracy in the WV measurements both over ocean and land surfaces.

In order to quantify the discrepancies between ECMWF model data and GOME-2A TCWV retrieval, in Fig. 9 we show the spatial distribution of the bias for daily co-located and (mostly) cloud-free measurements. The mean bias between the two data sets is 0.017 g cm^{-2} in February and 0.044 g cm^{-2} in August 2008.

In February the bias is overall very low. Any deviation below the typical scatter of water vapour data of 0.4 g cm^{-2} (i.e. the light green and blue areas on the plots) can be considered as a good agreement. As already mentioned, GOME-2 exhibits a number of dry and wet spots in south Africa and South America Amazonian regions, not visible in the ECMWF product, which is probably related to the very low number of co-locations in these regions, typically less than 8 measurements. Also problems of the ECMWF model data cannot be excluded, because it is unclear how many measurements went into the assimilated model at these locations. The differences over ocean, e.g. along the ITCZ and the Pacific Warm Pool region, on the other hand, seem to be related to the regions which present higher cloud top albedo and therefore an unsatisfactory removals of clouds: even though we consider only regions without severe cloud cover, some cloud effects are still present.

Relative large differences between GOME-2A and ECMWF data can be seen in August 2008. For example, in summer 2008, the humidity over the Sahara desert is much lower in GOME-2 data than expected in the ECMWF model data. Looking at the right panel of Fig. 9 we can see that the underestimation (blue regions denote negative bias) is located over desert regions like the above mentioned southern Sahara, as well as Saudi Arabia and eastern parts of North America. We also notice a negative bias in the region that goes from India till the east coast of China. In most places the bias is associated with high surface albedo values (in the range 0.3–0.5) and a high TCWV (i.e. large AMF).

AMTD
7, 3021–3073, 2014

A possible explanation of the discrepancies is that, because of absorbing aerosols over deserts, the surface albedo we measure there is lower than it's real values and therefore we underestimates the water vapour content (Fournier et al., 2006). In the future, we plan to further study the effect of the albedo database on the water vapour retrieval and refine this choice. However, we should have in mind that the determination of the "real" surface albedo over desert regions is still a field of discussion because of the uplifting of large amounts of dust, which lower the reflectivity (Herman et al., 1997; Torres et al., 1998). Finally, the scatter we observe in northern latitude ocean areas is mainly caused by atmospheric transport or motion which in general makes the validation of water vapour column more difficult with respect to other trace gas components.

5.2 Comparison with SSMIS TCWV observations

For the validation of GOME-2 H_2O total column with the Special Sensor Microwave Imager Sounder (SSMIS) we used data provided by the Remote Sensing System (REMSS, http://www.ssmi.com/ssmi/). The series of 7 Special Sensor Microwave/Imager (SSM/I) have been in orbit since 1987 on various platforms, predominantly those of the Defense Meteorological Satellite Programs (DMSP) F-platforms, and now the SSM/I series has been replaced by a combined imager/sounder called SSMIS. In this study we use SSMIS measurements of the F16 polar orbiting satellite between January 2007 and August 2013 in order to validate the TCWV GOME-2A data set. The SSMIS data products are produced as part of NASA's MEaSUREs Program and are generated using a unified, physically based algorithm to simultaneously retrieve ocean wind speed, atmospheric water vapor, cloud liquid water, and rain rate (Wentz, 1997). This algorithm is based on a model for the brightness temperature of the ocean and intervening atmosphere and is the product of 20 years of refinements, improvements and verifications.

Figure 10 shows the global monthly bias between GOME-2A and SSMIS observations in February and August 2008. As one can see, the land regions are masked in

AMTD
7, 3021–3073, 2014

the comparison, because the SSMIS data set is available only over ocean scenes, but microwave sensors can retrieve TCWV also in the presence of clouds and for night time satellite overpasses. If we evaluate the bias between the two data sets from monthly mean ECMWF data, we would find a larger and negative bias because of the cloud influence. Thus, as for ECMWF, we select only daily co-locations and we reject the SSMIS data if the corresponding GOME-2 measurement is contaminated by clouds (applying the cloud flag selection described in Sect. 3.1). We used only results from the descending F16 orbit from the daily binary SSMIS data files, so that on average SSMIS H_2O columns are measured 4.5 h before GOME-2 (GOME-2 flies Sun-synchronous with 9.30 a.m. equator crossing time, F16 around 5.03 p.m., but drifting – the ascending GOME-2 thus collocates with the descending F16). This selection minimizes the effect of temporal change and cloud contamination in the GOME-2 vs. SSMIS comparison.

In February 2008, we derive a small negative mean bias between GOME-2A and SSMIS ($-0.032\,g\,cm^{-2}$) (see Fig. 7). Looking at the top panel of Fig. 10, we can observe how the discrepancies are very small for most ocean regions, with the exception of some coastal areas, where the bias reaches values of the order of $\pm 0.5\,g\,cm^{-2}$. Nonetheless, we can observe a larger mean bias of about $0.097\,g\,cm^{-2}$ in August 2008 (bottom panel of Fig. 10). A positive bias is clearly visible in regions at high latitude, in particular the northern areas of the Atlantic and Pacific ocean and is the dominating cause for the pronounced seasonal component in SSMIS against GOME-2A validation results. Analyzing the cloud parameters retrieved by GOME-2A for daily co-located measurements, we found that high values of the bias are typically associated with higher cloud fractions. We can therefore argue that residual cloud effects influence the GOME-2 retrieval. On the other hand, we do not find any clear dependence of the bias on the cloud top height parameter, as claimed, for example, in the validation between radiosonde and SCIAMACHY data retrieved with the AMC-DOAS algorithm (du Piesanie et al., 2013).

AMTD
7, 3021–3073, 2014

Among the limitations of the SSMIS data, on the other hand, we should mention that in situations with high rain content the retrieval is not possible and, more important, the model and algorithm for the retrieval are calibrated using an in-situ database containing overpasses of buoys and radiosonde sites. The accuracy of the TCWV product depends on the quality of these observations, and not all the regions and atmospheric situations may be equally represented in the training data set (Andersson et al., 2010). It was already shown that the maximum bias between satellite and ship data (of about $0.25\,g\,kg^{-1}$) was found precisely over the North Ocean Atlantic during the summer season (Bentamy et al., 2003). Also, depending on location and season, systematic differences of atmospheric humidity of about 1 % for 1 h time difference between the GOME-2A and SSMIS retrieval might be expected, and in regions with a particularly high intradaily variability, as for instance over the North Atlantic, they can be even larger.

5.3 Comparison with the SSM/I + MERIS TCWV data set

The cross-comparison of the GOME-2 product vs. the combined SSM/I + MERIS GlobVapour data set for February and August 2008 is shown in Fig. 11. The MERIS TCWV algorithm (Lindstrot et al., 2012) is used above land and coastal areas and these measurements are combined with SSM/I data (Fennig et al., 2012) over ocean to provide a global coverage. Since MERIS retrieves data only during daytime and at a fixed equator crossing time (10.00 a.m.), in order to provide a consistent data set, also the SSM/I products were created from morning overpasses (descending path) of the F13 and F14 satellites. In the framework of the GlobVapour project, an improved version of the HOAPS algorithm has been developed for the SSM/I TCWV retrieval, and the bias between the SSM/I and MERIS data sets has been assessed by comparing the results of both retrievals over sun-glint areas, in order to assure a smooth transition from ocean to land and island sites (Schröder et al., 2012b). For the validation with GOME-2 TCWV, we use gridded Level 3 data, which have a spatial resolution of $0.5^{\circ} \times 0.5^{\circ}$, in the period January 2007–December 2008.

AMTD
7, 3021–3073, 2014

Figure 11 shows that the agreement between GlobVapour data and GOME-2 data over land seems to be somewhat better than over ocean. The difference plot in February 2008 (top panel) is quite noisy and the GOME-2 data over ocean tend to be lower than the corresponding SSM/I + MERIS monthly mean. This is in line with the results we obtain from the comparison with SSMIS data for the same month, but the bias presents larger values because the SSM/I observations we use also contain measurements with large cloud cover (we use monthly mean data instead of daily co-locations). An interesting ocean area is the one west of Central America and Colombia and coast of Africa, where we have positive differences, not seen in the ECMWF comparison (Sect. 4.1) and associated to higher cloud top albedo values. Over the continents the agreement between both data sets is generally very good. A specific advantage of the MERIS instrument is the very high spatial resolution (1 km × 1.2 km in the reduced resolution mode) and therefore the ability to retrieve sharp gradient in water vapour abundance with great accuracy. We can observe extended regions with very small biases, close to zero, especially in Asia and Africa. Exceptions are found in some specific small regions where GOME-2 columns are higher than the MERIS values. An over-estimation of water vapour content by GOME-2 (or underestimation by SSM/I + MERIS) seems to occur preferably over Europe and the western part of North America. Major differences are located in coastal areas, where neither SSM/I, nor MERIS provide accurate estimates. For MERIS, this is due to the weak reflectance of the ocean in the near infrared and on the resulting uncertainties introduced by the unknown contribution of aerosol scattering and absorption, while SSM/I measurements cannot be used in case of relative large footprint contaminated by land. We do not detect these potentially important differences in the comparison with ERA-Interim reanalysis data, and thus it is also not clear whether the discrepancies we observe at high latitude are real or result from difficulties with the retrieval over ice-covered regions (Schröder et al., 2012c). Finally, as for GOME-2, the quality of the MERIS TCWV retrieval algorithm strongly depends on the reliability of the cloud screening procedure, and we can expect a weak dry bias, where the cloud detections fail.

AMTD
7, 3021–3073, 2014

The average bias for the validations GOME-2A–SSM/I + MERIS in February 2008 is negative ($-0.021\,g\,cm^{-2}$), while we found a small and positive bias ($0.01\,g\,cm^{-2}$) in August 2008. As we have already seen in Fig. 7, also for this data set we can observe a systematic variation in the bias between winter and summer months, with lower GOME-2 values in the NH winter season and higher data in summer, but the amplitude of this variation is smaller with respect to the validation against SSMIS. The different temporal selection (monthly means as opposed to daily co-located measurements), and consequently the different cloud selections applied to the GOME-2 and SSM/I measurements, has the effect of decreasing the bias in the ocean regions. However, the smaller seasonal variability is due prevalently to the opposite and complementary bias trends over ocean and continents (already observed in Schröder and Schneider, 2012), so that in the NH winter months we observe preferably negative bias over sea and positive bias over land. In the NH summer month (see bottom panel of Fig. 11), on the other hand, the MERIS data tend to be more wet than the corresponding GOME-2A data, with a large bias in the south-east Asia, the southern Sahara and part of the Saudi Arabia and North America. The discrepancies are positively correlated with GOME-2A regions with high surface albedo. In previous studies (Lindstrot at al., 2012), also a potential underestimation of the absorption at 900 nm was identified as a possible source of a wet bias in the MERIS data set.

An orthogonal regression analysis of the scatter between GOME-2 and SSM/I + MERIS measurements shows a good correlation between both data sets. This analysis is particularly interesting to assess the consistency between the monthly mean data sets. We found an almost ideal slope of 0.981 and 1.006 in February and August 2008 (see top and bottom panel of Fig. 12), respectively. Also the offset is very small especially for the summer comparison ($-4 \times 10^{-4}\,g\,cm^{-2}$). Although the majority of data shows very good correlation, MERIS mid value water columns (i.e., 1 to $3\,g\,cm^{-2}$) are often lower than the GOME co-located products. In August 2008 the largest scatter occurs for values around $2\,g\,cm^{-2}$, which are observed in the transition zone between tropics and extra-tropics, where large natural variability is observed.

AMTD
7, 3021–3073, 2014

6 Summary and conclusions

In this paper, we present the algorithm for the retrieval of the water vapour total column from the Global Ozone Monitoring Experiment-2 (GOME-2) on board of the MetOp-A and MetOp-B platforms and we perform an analysis and evaluation of this data set against independent satellite observations and forecast data.

The operational GOME-2 H_2O column product used in this study is developed in the framework of EUMETSAT's O3M-SAF project in co-operation with MPI-C Mainz and DLR Oberpfaffenhofen, and generated by DLR using the UPAS environment and the GDP 4.7 algorithm. The retrieval algorithm is based on a classical DOAS method to obtain the trace gas slant column. Subsequently, the vertical column is derived, making use of the simultaneously measured O_2 absorption and radiative transfer calculations. This procedure is robust (it provides similar sensitivity over land and ocean), very fast and, in contrast to other satellite retrieval methods, is independent from a priori assumptions on atmospheric properties.

In GDP 4.7, the quality of the GOME-2 H_2O column has been enhanced with respect to two major aspects. We further investigate and improve the cloud selection criteria used in the retrieval algorithm and we eliminated the dependency of the data set on the viewing angle conditions by consistently applying a distinct empirical correction for land and ocean surfaces, both to GOME-2/MetOp-A (GOME-2A) and to GOME-2/MetOp-B (GOME-2B) measurements. We also present exemplary results from about 8 months measurements of the new GOME-2 MetOp-B instrument, launched on 17 October 2012, and an inter-comparison with the GOME-2/MetOp-A data for the overlap period. We found that the GOME-2B water vapour total columns are only slightly wetter than the GOME-2A measurements and present a small, positive bias of about $0.01\,\mathrm{g\,cm^{-2}}$ (less than 1 %), when averaging all the results for the December 2012 to August 2013 time period. Latitudinal averaged differences can be as large as $0.117\,\mathrm{g\,cm^{-2}}$ at low latitudes, because of the reduced overlap between the GOME-2A and GOME-2B orbits is lower in the tropics.

AMTD
7, 3021–3073, 2014

Assimilated data and independent satellite observations are used to document the geophysical consistency of the H_2O column data. Total column water vapour estimates from the GOME-2A and GOME-2B instruments are then collocated and compared with the SSMIS satellite F16 measurements and with model data from the European Centre for Medium Range Weather Forecast (ECMWF) during the full period 2007–2013. We then conclude our extensive validation using comparisons against a combined SSM/I + MERIS data set (as developed in the framework of the ESA DUE GlobVapour project) in 2007 and 2008.

Within our analysis, we found a surprisingly good agreement between GOME-2 type instruments and the four independent data sets analyzed here, with a mean bias within $\pm 0.035\,\mathrm{g\,cm^{-2}}$ for the time interval January 2007–August 2013. The annual variability over land and coastal areas is low, but over ocean we observe a clear seasonal cycle with highest values during NH summer. Slightly lower than in summer, and negative biases are found in the NH winter months. These variations can mainly be related to the impact of clouds on the accuracy of the GOME-2 observations and to the different sampling statistics of the instruments.

Global monthly averaged differences between the combined SSM/I + MERIS data sets and GOME-2 data are within a $\pm 0.03\,\mathrm{g\,cm^{-2}}$ range, with GOME-2A data typically drier than MERIS data over land areas with high humidity and a relatively large surface albedo, a circumstance which may indicate an influence of the surface albedo correction in the AMF calculation. Collocated GOME-2A data present a mean bias of $0.017\,\mathrm{g\,cm^{-2}}$ (0.4 %) and 0.044 (1.1 %) with TCWV data from the latest ECMWF ERA Intermin reanalysis in February and August 2008, respectively. We discuss possible causes for the bias and demonstrate the value of the GOME-2 data record using these two exemplary months as representative of the global distribution of the bias during NH winter and summer. In August 2008 the correlation between the GOME observations and the SSMIS F16 satellite measurements yield an average bias of $0.097\,\mathrm{g\,cm^{-2}}$, and the differences in TCWV measured by the two systems is dominated by residual clouds effects and the diurnal variability of the WV data over the North Atlantic Ocean.

AMTD
7, 3021–3073, 2014

GOME-2/MetOp-A and GOME-2/MetOp-B total column water vapour obtained with the GDP 4.7 algorithm continues the GOME and SCIAMACHY time series started in 1995. With the launch of the new GOME-2/MetOp-C instrument, the GOME-type data record will be further extended to cover a period of at least 25 years WV measurements. This unique data set has now reached high accuracy and stability and is expected to provide important information on long-term changes of our atmosphere.

Acknowledgements. Development of the GOME-2 water vapour products and their validation has been funded by the O3M-SAF project with EUMETSAT and national contributions. The authors thank the DFD colleagues S. Kiemle, K. H. Seitz, T. Padsuren and M. Schwinger who are responsible for day-to-day operations of the O3M-SAF facility at DLR. We thank EUMETSAT for the ground segment interfacing work with the O3M-SAF systems and for the provision of GOME-2 Level 1 products.

The service charges for this open access publication have been covered by a Research Centre of the Helmholtz Association.

References

Andersson, A., Fennig, K., Klepp, C., Bakan, S., Graßl, H., and Schulz, J.: The Hamburg Ocean Atmosphere Parameters and Fluxes from Satellite Data – HOAPS-3, Earth Syst. Sci. Data, 2, 215–234, doi:10.5194/essd-2-215-2010, 2010.

Bauer, P. and Schlüssel, P.: Rainfall, total water, ice water, and water vapor over sea from polarized microwave simulations and Special Sensor Microwave/Imager data, J. Geophys. Res., 98, 20737–20759, 1993.

Bentamy, A., Katsaros, K. B., Mestas-Nunez, A. M., Drennan, W. M., Forde, B. E., and Roquet, H.: Satellite estimates of wind speed and latent heat flux over the global oceans, J. Climate, 16, 637–655, 2003.

Bevis, M., Businger, S., Herring, T. A., Rocken, C., Anthes, R. A., and Ware, R. H.: GPS meteorology: remote sensing of atmospheric water-vapor using the Global Positioning System, J. Geophys. Res., 97, 15787–15801, 1992.

AMTD
7, 3021–3073, 2014

Bevis, M., Businger, S., Chiswell, S., Herring, T. A., Anthes, R. A., Rocken, C., and Ware, R. H.: GPS meteorology – mapping zenith wet delays onto precipitable water, J. Appl. Meteorol., 33, 379–386, 1994.

Bovensmann, H., Burrows, J. P., Buchwitz, M., Frerick, J., Noël, S., Rozanov, V. V., Chance, K. V., and Goede, A. H. P.: SCIAMACHY – mission objectives and measurement modes, J. Atmos. Sci., 56, 127–150, 1999.

Burrows, J. P., Weber, M., Buchwitz, M., Rozanov, V., Ladstätter-Weißenmayer, A., Richter, A., de Beek, R., Hoogen, R., Bramstedt, K., Eichmann, K.-U., Eisinger, M., and Perner, D.: The Global Ozone Monitoring Experiment (GOME): mission concept and first scientific results, J. Atmos. Sci., 56, 151–175, 1999.

Callies, J., Corpaccioli, E., Eisinger, M., Hahne, A., and Lefebvre, A.: GOME-2 – MetOp's second generation sensor for operational ozone monitoring, ESA Bull.-Eur. Space, 102, 28–36, 2000.

Casadio, S., Zehner, C., Piscane, G., and Putz, E.: Emperical Retrieval of Atmospheric Air-mass factor (ERA) for the measurement of water vapour vertical content using GOME data, Geophys. Res. Lett., 27, 1483–1486, 2000.

Cox, C. and Munk, W. H.: Measurements of the roughness of the sea surface from photographs of the sun's glitter, J. Opt. Soc. Am., 44, 838–850, 1954.

Dai, A., Wang, J., Ware, R. H., and Hove, T. V.: Diurnal variation in water vapor over North America and its implications for sampling errors in radiosonde humidity, J. Geophys. Res., 107, ACL11.1–ACL11.14, doi:10.1029/2001JD000642, 2002.

Dee, D. P., Uppala, S. M., Simmons, A. J., Berrisford, P., Poli, P., Kobayashi, S., Andrae, U., Balmaseda, M. A., Balsamo, G., Bauer, P., Bechtold, P., Beljaars, A. C. M., van de Berg, L., Bidlot, J., Bormann, N., Delsol, C., Dragani, R., Fuentes, M., Geer, A. J., Haimberger, L., Healy, S. B., Hersbach, H., Hólm, E. V., Isaksen, L., Kållberg, P., Köhler, M., Matricardi, M., McNally, A. P., Monge-Sanz, B. M., Morcrette, J.-J., Park, B.-K., Peubey, C., de Rosnay, P., Tavolato, C., Thépaut, J.-N., and Vitart, F.: The ERA-Interim reanalysis: configuration and performance of the data assimilation system, Q. J. Roy. Meteorol. Soc., 137, 553–597, 2011a.

Dee, D., Berrisford, P., Bosilovich, M. G., Chelliah, M., Compo, G., Ebita, A., Jones, P. D., Kobayashi, S., Kumar, A., Rutledge, G., Saha, S., Sato, H., Simmons, A., Smith, C., and Vose, R.: The use of reanalysis data for monitoring the state of the climate [in "The State of the Climate in 2010"], B. Am. Meteorol. Soc., 92, S34–S35, 2011b.

AMTD
7, 3021–3073, 2014

Deutschmann, T., Beirle, S., Frieß, U., Grzegorski, M., Kern, C., Kritten, L., Platt, U., Pukite, J., Wagner, T., Werner, B., and Pfeilsticker, K.: The Monte Carlo Atmospheric Radiative Transfer Model McArtim: introduction and validation of Jacobians and 3D features, J. Quant. Spectrosc. Ra., 112, 1119–1137, doi:10.1016/j.jqsrt.2010.12.009, 2011.

du Piesanie, A., Piters, A. J. M., Aben, I., Schrijver, H., Wang, P., and Noël, S.: Validation of two independent retrievals of SCIAMACHY water vapour columns using radiosonde data, Atmos. Meas. Tech. Discuss., 6, 665–702, doi:10.5194/amtd-6-665-2013, 2013.

Fennig, K., Andersson, A., Bakan, S., Klepp, C., and Schroeder, M.: Hamburg Ocean Atmosphere Parameters and Fluxes from Satellite Data – HOAPS 3.2 – monthly means/6-hourly composites, Satellite Application Facility on Climate Monitoring, doi:10.5676/EUM_SAF_CM/HOAPS/V001, 2012.

Fournier, N., Stammes, P., de Graaf, M., van der A, R., Piters, A., Grzegorski, M., and Kokhanovsky, A.: Improving cloud information over deserts from SCIAMACHY Oxygen A-band measurements, Atmos. Chem. Phys., 6, 163–172, doi:10.5194/acp-6-163-2006, 2006.

Gaffen, D. J., Barnett, T. P., and Elliott, W. P.: Space and time scales of global tropospheric moisture, J. Climate, 4, 989–1008, 1991.

Gomer, T., Brauers, T., Heintz, F., Stutz, J., and Platt, U.: MFC user manual, version 1.98, inhouse publication, Institut für Umweltphysik, University of Heidelberg, Germany, 1993.

Grossi, M., Kalakoski, N., and Valks, P.: O3M SAF ORR VALIDATION REPORT, SAF/O3M/DLR/ORR/H2O, Issue 01/2013, 2013.

Grzegorski, M.: Cloud Retrieval from UV/VIS Satellite Instruments (SCIAMACHY and GOME), Ph.D. thesis, University of Heidelberg, 2009.

Grzegorski, M., Frankenberg, C., Platt, U., Wenig, M., Fournier, N., Stammes, P., and Wagner, T.: Determination of cloud parameters from SCIAMACHY data for the correction of tropospheric trace gases, in: ESA-Publication SP-572 (CD-ROM), Proceedings of the ENVISAT & ERS Symposium, 6–10 September 2004, Salzburg, Austria, 1658, 1664, 2004.

Herman, J. R., Bhartia, P. K., Torres, O., Hsu, C., Seftor, C., and Celarier, E. A.: Global distributions of UV-absorbing aerosols from Nimbus-7 TOMS data, J. Geophys. Res., 102, 16911–16922, 1997.

Hovila, D., Kiemle, J. S., Tuinder, O., Joench-Soerensen, H., and Karcher, F.: Product Requirements Document, SAF/O3M/FMI/RQ/PRD/001/Rev. 06, 2008.

Kalakoski, N., Wagner, T., Mies, K., Beirle, S., Slijkhuis, S., and Loyola, D.: O3M SAF Validation Report, Offline Total Water Vapour, SAF/O3M/FMI/VR/H2O/111, 2011.

AMTD
7, 3021–3073, 2014

Koelemeijer, R. B. A., Haan, J. F. D., and Stammes, P.: A database of spectral surface reflectivity in the range 335–772 nm derived from 5.5 years of GOME observations, J. Geophys. Res., 108, D24070, doi:10.1029/2002JD002429, 2003.

Lang, R., Williams, J. E., van der Zande, W. J., and Maurellis, A. N.: Application of the Spectral Structure Parameterization technique: retrieval of total water vapor columns from GOME, Atmos. Chem. Phys., 3, 145–160, doi:10.5194/acp-3-145-2003, 2003.

Lang, R., Casadio, S., Maurellis, A. N., and Lawrence, M. G.: Evaluation of the GOME Water Vapor Climatology 1995–2002, J. Geophys. Res., 112, D12110, doi:10.1029/2006JD008246, 2007.

Learner, R., Schermaul, R., Tennyson, J., Zobov, N., Ballard, J., Newnham, D., and Wickett, M.: Measurement of H_2O Absorption Cross-Sections for the Exploitation of GOME data, ESTEC Contract No 13312/9/NL/SF, Final Presentation, 7919, 2000.

Li, Z., Fielding, E. J., Cross, P., and Muller, J.-P.: Interferometric synthetic aperture radar atmospheric correction: MEdium Resolution Imaging Spectrometer and Advanced Synthetic Aperture Radar integration, Geophys. Res. Lett., 33, L06816, doi:10.1029/2005GL025299, 2006.

Lichtenberg, G., Bovensmann, H., Van Roozendael, M., Doicu, A., Eichmann, K.-U., Hess, M., Hrechanyy, S., Kokhanovsky, A., Lerot, C., Noel, S., Richter, A., Rozanov, A., Schreier, F., and Tilstra, L. G.: SCIAMACHY Offline Level 1b-2 Processor ATBD (ENV-ATB-QWG-SCIA-0085, issue 1A), 2010.

Lindstrot, R., Preusker, R., Diedrich, H., Doppler, L., Bennartz, R., and Fischer, J.: 1D-Var retrieval of daytime total columnar water vapour from MERIS measurements, Atmos. Meas. Tech., 5, 631–646, doi:10.5194/amt-5-631-2012, 2012.

Loyola, D., Valks, P., Ruppert, T., Richter, A., Wagner, T., Thomas, W., van der A, R., and Meisner, R.: The 1997 El Niño impact on clouds, water vapour, aerosols and reactive trace gases in the troposphere, as measured by the Global Ozone Monitoring Experiment, Adv. Geosci., 6, 267–272, doi:10.5194/adgeo-6-267-2006, 2006.

Loyola, D., Thomas, W., Livschitz, Y., Ruppert, T., Albert, P., and Hollmann, R.: Cloud properties derived from GOME/ERS-2 backscatter data for trace gas retrieval, IEEE T. Geosci. Remote, 45, 2747–2758, 2007.

Loyola, D., Thomas, W., Spurr, R., and Mayer, B.: Global patterns in daytime cloud properties derived from GOME backscatter UV-VIS measurements, Int. J. Remote Sens., 31, 4295–4318, 2010.

AMTD
7, 3021–3073, 2014

Loyola, D., Koukouli, M. E., Valks, P., Balis, D. S., Hao, N., Van Roozendael, M., Spurr, R. J. D., Zimmer, W., Kiemle, S., Lerot, C., and Lambert, J.-C: The GOME-2 total column ozone product: retrieval algorithm and ground-based validation, J. Geophys. Res., 116, D07302, doi:10.1029/2010JD014675, 2011.

Maurellis, A. N., Lang, R., Van der Zande, W. J., Ubachs, W., and Aben, I.: Precipitable Water Column Retrieval from GOME, Geophys. Res. Lett., 27, 903–906, 2000.

Mieruch, S., Noël, S., Bovensmann, H., and Burrows, J. P.: Analysis of global water vapour trends from satellite measurements in the visible spectral range, Atmos. Chem. Phys., 8, 491–504, doi:10.5194/acp-8-491-2008, 2008.

Mieruch, S., Schröder, M., Noël, S., and Schulz, J.: Comparison of monthly means of global total column water vapor retrieved from independent satellite observations, J. Geophys. Res., 115, D23310, doi:10.1029/2010JD013946, 2010.

Minschwaner, K. and Dessler, A. E.: Water vapor feedback in the tropical upper troposphere: model results and observations, J. Climate, 17, 1272–1282, 2004.

Munro, R., Eisinger, M., Anderson, C., Callies, J., Corpaccioli, E., Lang, R., Lefebvre, A., Livschitz, Y., and Perez Albinana, A.: GOME-2 on MetOp: from in-orbit verification to routine operations, in: Proceedings of EUMETSAT Meteorological Satellite Conference, Helsinki, Finland, 12–16 June 2006, 2006.

Noel, S., Buchwitz, M., Bovensmann, H., Hoogen, R., and Burrows, J. P.: Atmospheric Water Vapor Amounts Retrieved from GOME Satellite Data, Geophys. Res. Lett., 26, 1841–1844, 1999.

Noël, S., Mieruch, S., Bovensmann, H., and Burrows, J. P.: Preliminary results of GOME-2 water vapour retrievals and first applications in polar regions, Atmos. Chem. Phys., 8, 1519–1529, doi:10.5194/acp-8-1519-2008, 2008.

Platt, U.: Differential optical absorption spectroscopy (DOAS), in: Air Monitoring by Spectroscopic Techniques, Chem. Anal. Ser., Vol. 127, edited by: Sigrist, M. W., John Wiley, Hoboken, NJ, 27–84, 1994.

Rocken, C., Ware, R. H., Van Hove, T., Solheim, F., Alber, C., and Johnson, J.: Sensing atmospheric water vapor with the Global Positioning System, Geophys. Res. Lett., 20, 2631–2634, 1993.

Rocken, C., Van Hove, T., and Ware, R. H.: Near real-time GPS sensing of atmospheric water vapor, Geophys. Res. Lett., 24, 3221–3224, 1997.

AMTD
7, 3021–3073, 2014

Rocken, C., Kuo, Y.-H., Schreiner, W., Hunt, D., Sokolovskiy, S., and McCormick, C.: COSMIC system description, Terr. Atmos. Ocean. Sci., 11, 21–52, 2000.

Rothman, L. S., Gordon, I. E., Barbe, A., Benner, D. Chris, Bernath, P. F., Birk, M., Boudon, V., Brown, L. R., Campargue, A., Champion, J.-P., Chance, K., Coudert, L. H., Dana, V., Devi, V. M., Fally, S., Flaud, J.-M., Gamache, R. R., Goldman, A., Jacquemart, D., Kleiner, I., Lacome, N., Lafferty, W. J., Mandin, J.-Y., Massie, S. T., Mikhailenko, S. N., Miller, C. E., Moazzen-Ahmadi, N., Naumenko, O. V., Nikitin, A. V., Orphal, J., Perevalov, V. I., Perrin, A., Predoi-Cross, A., Rinsland, C. P., Rotger, M., Šimeèková, M., Smith, M. A. H., Sung, K., Tashkun, S. A., Tennyson, J., Toth, R. A., Vandaele, A. C., and Vander Auwera, J.: The HITRAN 2008 molecular spectroscopic database, J. Quant. Spectrosc. Ra., 110, 533–72, 2009.

Schröder, M. and Schneider, N.: DUE GLOBVAPOUR Product Validation Report (PVR) Cross-Comparison, Issue 1, Revision 1, 21 August 2012, 2012.

Schröder, M., Slijkhuis, S., and Wagner, T.: DUE GLOBVAPOUR Algorithm Theoretical Baseline Document (ATBD) for L3 GOME+SCIAMACHY+GOME-2, Issue 3, Revision 0, 19 January 2012, 2012a.

Schröder, M., Lindstrot, R., and Schneider, N.: DUE GLOBVAPOUR Algorithm Theoretical Baseline Document (ATBD) for L3 SSMI + MERIS, Issue 3, Revision 0, 19 January 2012, 2012b.

Schröder, M., Saunders, R., and Ringer, M.: DUE GLOBVAPOUR Scientific Exploitation Plan (SEP), Issue 1, Revision 0, 17 April 2012, 2012c.

Slijkhuis, S., Beirle, S., Kalakoski, N., Mies, K., Wagner, T., Noël, S., and Schulz, J.: Comparison of H_2O retrievals from GOME and GOME-2, in: Proc. EUMETSATP.55, 2009.

Solomon, S., Miller, H. L., Smith, J. P., Sanders, R. W., Mount, G. H., Schmeltekopf, A. L., and Noxon, J. F: Atmospheric NO_3 1. Measurement technique and the annual cycle, J. Geophys. Res., 94, 11041–11048, 1989.

Torres, O., Bhartia, P. K., Herman, J. R., Ahmad, Z., and Gleason, J. F.: Derivation of aerosol properties from satellite measurements of backscattered ultraviolet radiation: theoretical basis, J. Geophys. Res., 103, 17099–17110, 1998.

Trenberth, K. E. and Stepaniak, D. P.: Co-variability of components of poleward atmospheric energy transports on seasonal and interannual timescales, J. Climate, 16, 3691–3705, 2003.

AMTD
7, 3021–3073, 2014

Trenberth, K. E., Smith, L., Qian, T., Dai, A., and Fasullo, J.: Estimates of the global water budget and its annual cycle using observational and model data, J. Hydrometeorol., 8, 758–769, 2007.

Valks, P., Loyola, D., Hao, N., Rix, M., and lijkhuis, S. S.: Algorithm Theoretical Basis Document for GOME-2 Total Column Products of Ozone, Minor Trace Gases and Cloud Properties (GDP 4.5 for O3M-SAF OTO and NTO), DLR/GOME-2/ATBD/01, Iss./Rev.: 2/GG, 2012.

Van Roozendael, M., Fayt, C., Lambert, J.-C., Pundt, I., Wagner, T., Richter, A., and Chance, K.: Development of a bromine oxide product from GOME, in: Proceedings of the European Symposium on Atmospheric Measurements From Space (ESAMS 99), 18–22 January, ESTEC, Noordwijk, Netherlands, Rep. WPP-161, 543–547, Eur. Space Agency, Noordwijk, Netherlands, 1999.

Wagner, T., Otten, C., Pfeilsticker, K., Pundt, I., and Platt, U.: DOAS moonlight observation of atmospheric NO_3 and NO_2 in the Arctic winter, Geophys. Res. Lett, 27, 3441–3444, 2000.

Wagner, T., Heland, J., Zöger, M., and Platt, U.: A fast H_2O total column density product from GOME – Validation with in-situ aircraft measurements, Atmos. Chem. Phys., 3, 651–663, doi:10.5194/acp-3-651-2003, 2003.

Wagner, T., Beirle, S., Grzegorski, M., Sanghavi, S., and Platt, U.: El-Nino induced anomalies in global data sets of total column precipitable water and cloud cover derived from GOME on ERS-2, J. Geophys. Res., 110, D151642, doi:10.1029/2005JD005972, 2005.

Wagner, T., Beirle, S., Grzegorski, M., and Platt, U.: Global trends (1996–2003) of total column precipitable water observed by Global Ozone Monitoring Experiment (GOME) on ERS-2 and their relation to near-surface temperature, J. Geophys. Res., 111, D12102, doi:10.1029/2005JD006523, 2006.

Wagner, T., Beirle, S., Deutschmann, T., Grzegorski, M., and Platt, U.: Satellite monitoring of different vegetation types by differential optical absorption spectroscopy (DOAS) in the red spectral range, Atmos. Chem. Phys., 7, 69–79, doi:10.5194/acp-7-69-2007, 2007.

Wagner, T., Beirle, S., and Deutschmann, T.: Three-dimensional simulation of the Ring effect in observations of scattered sun light using Monte Carlo radiative transfer models, Atmos. Meas. Tech., 2, 113–124, doi:10.5194/amt-2-113-2009, 2009.

Wagner, T., Beirle, S., and Mies, C.: Description of the MPI-Mainz H_2O retrieval (Version 5.0, March 2011), 2011.

AMTD
7, 3021–3073, 2014

Wang, J., Cole, H. L., Carlson, D. J., Miller, E. R., Beierle, K., Paukkunen, A., and Laine, T. K.: Corrections of humidity measurement errors from the Vaisala RS80 radiosonde – application to TOGA COARE data, J. Atmos. Ocean. Tech., 19, 981–1002, 2002.

Wentz, F. J.: A well-calibrated ocean algorithm for SSM/I, J. Geophys. Res., 102, 8703–8718, 1997.

Wentz, F. J.: SSM/I Version-7 Calibration Report, report number 011012, Remote Sensing Systems, Santa Rosa, CA, 46 pp., 2013.

AMTD
7, 3021–3073, 2014

Table 1. Summary of GOME-type instruments characteristics. The main improvement of GOME-2 compared to its predecessor GOME/ERS-2 are clearly visible.

Sensor Satellite	GOME ERS-2	SCIAMACHY ENVISAT	GOME-2 MetOp-A	GOME-2 MetOp-B
Data period	Jun 1995–present	Aug 2002–Apr 2012	Jan 2007–present	Dec 2012–present
Spectral coverage	240–790 nm	240–2380 nm	240–790 nm	240–790 nm
Ground pixel size	320 km × 40 km	60 km × 30 km	80 km × 40 km– 40 km × 40 km[a]	80 × 40 km
Swath width	960 km	960 km	1920–960 km[a]	1920 km
Equator crossing time	10.30 a.m. LT	10.00 a.m. LT	9.30 a.m. LT	9.30 a.m. LT
Global coverage	3 days[b]	6 days	1.5 days	1.5 days

[a] GOME-2A tandem operation since 15 July 2013.
[b] GOME global coverage lost in June 2003.

AMTD
7, 3021–3073, 2014

Table 2. Statistics of the time period January 2007–August 2013. Bias and RMSE refer to the average difference GOME-2A – DATA.

Data	Bias [g cm^{-2}]	RMSE [g cm^{-2}]
GOME-2A – ECMWF	0.034 ± 0.014	0.522 ± 0.045
GOME-2A – SSMIS	0.028 ± 0.052	0.644 ± 0.046
GOME-2A – SSM/I + MERIS	−0.005 ± 0.020	0.409 ± 0.048
GOME-2B – ECMWF	0.082 ± 0.012	0.539 ± 0.052
GOME-2B – SSMIS	0.088 ± 0.057	0.654 ± 0.050

AMTD
7, 3021–3073, 2014

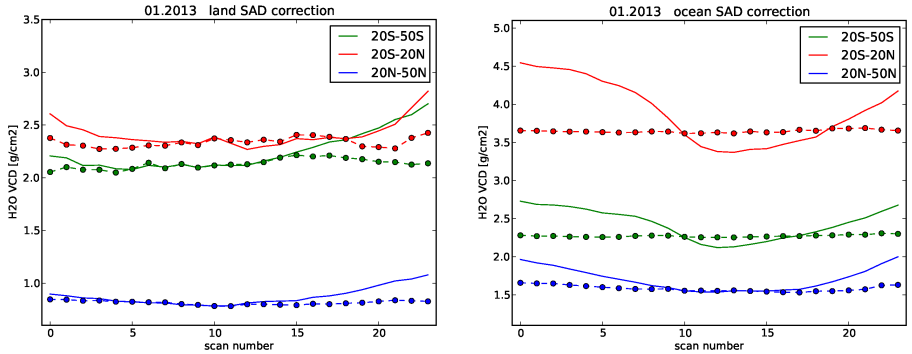

Fig. 1. H_2O VCD as a function of the number of the pixel index within the scan (0 = East, 24 = West) averaged in different latitude bands (20–50° S, 20° S–20° N, 20–50° N) before (solid line) and after (dashed line with points) the Scan Angle Dependency correction for January 2013. We show separately the empirical correction applied over land measurements (left panel) and over ocean measurements (right panel).

AMTD
7, 3021–3073, 2014

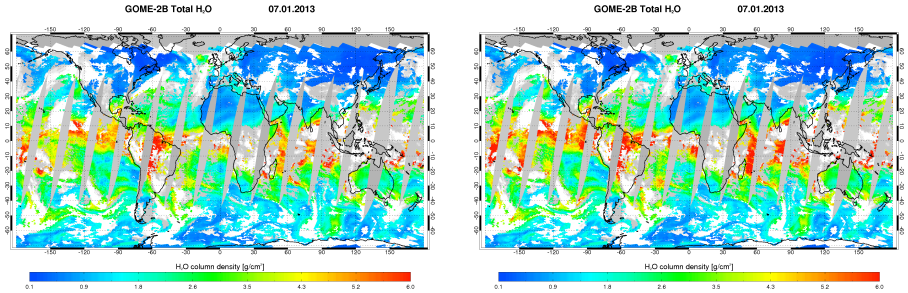

Fig. 2. H_2O vertical columns derived from GOME-2B measurements for the 7 January 2013 using the SAD correction (on the left) and without the SAD correction (on the right). Only cloud-screened data corresponding to solar zenith angles smaller than 87° are shown.

AMTD
7, 3021–3073, 2014

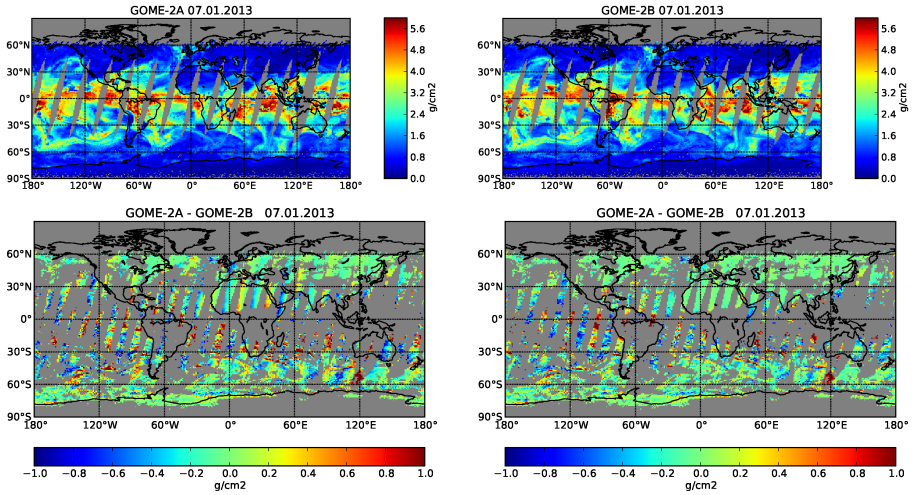

Fig. 3. Top panels: daily averages of total H_2O vertical columns from GOME-2A and GOME-2B for the 7 January 2013 with SAD correction applied. Only data corresponding to solar zenith angles lower than 87° are used. GOME-2A and GOME-2B measurements are separated by approximately 48 min in time. Bottom panels: geographical distribution of the differences between GOME-2A and GOME-2B water vapour column for the 7 January 2013 when the SAD correction is applied to the two data sets (right panel, GDP 4.7) and without SAD correction (left panel, GDP 4.6). In the plot are shown cloud-free co-located measurements.

AMTD
7, 3021–3073, 2014

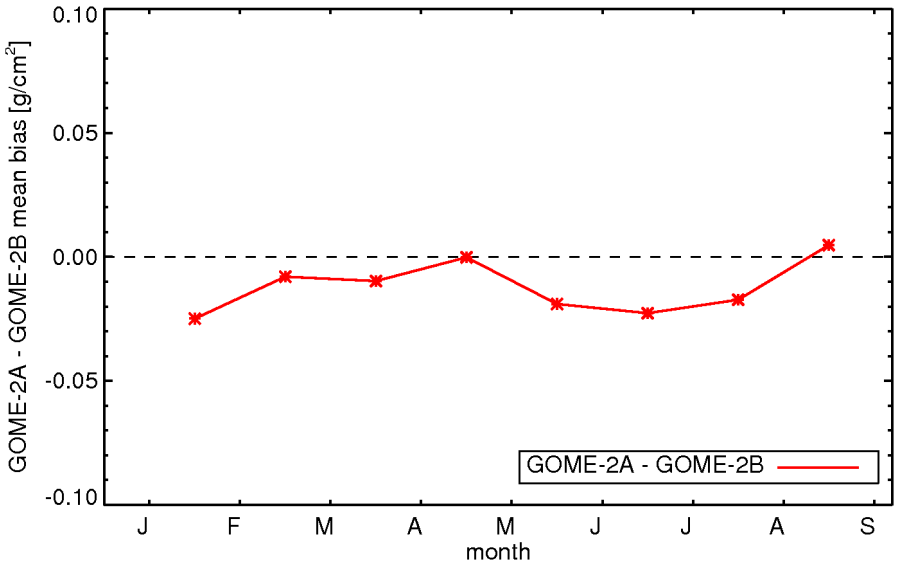

Fig. 4. Global monthly mean H_2O total column bias between GOME-2/MetOp-A and GOME-2/MetOp-B for the period January 2013–August 2013.

AMTD
7, 3021–3073, 2014

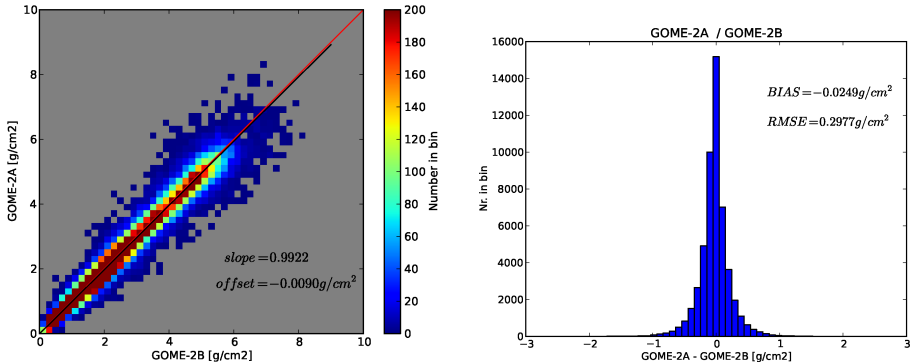

Fig. 5. Left panel: scatter plot of GOME-2A monthly mean total columns against GOME-2B monthly mean total columns, for January 2013 and cloud-free sky. The slope of the orthogonal regression is 0.992 with an offset of $-0.009\,\mathrm{g\,cm^{-2}}$. Right panel: histogram of the difference GOME-2A – GOME-2B, for the points in the scatter plot. The mean bias is $-0.0249\,\mathrm{g\,cm^{-2}}$ with a root mean square error of $0.297\,\mathrm{g\,cm^{-2}}$ and a negative skewness.

AMTD
7, 3021–3073, 2014

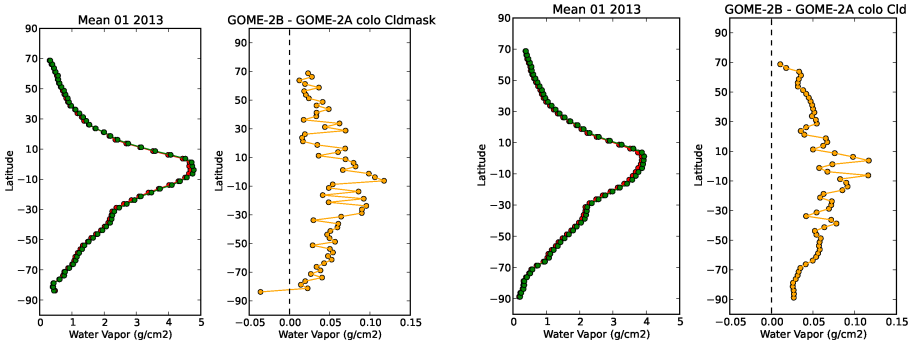

Fig. 6. Zonal mean H_2O total column from GOME-2A (green points) and from GOME-2B (red points) as a function of latitude for January 2013 and bias between GOME-2B and GOME-2A monthly averaged H_2O column. The results refer to daily co-located GOME-2A and GOME-2B measurements with cloud mask (left plot) and without cloud mask (right plot).

AMTD
7, 3021–3073, 2014

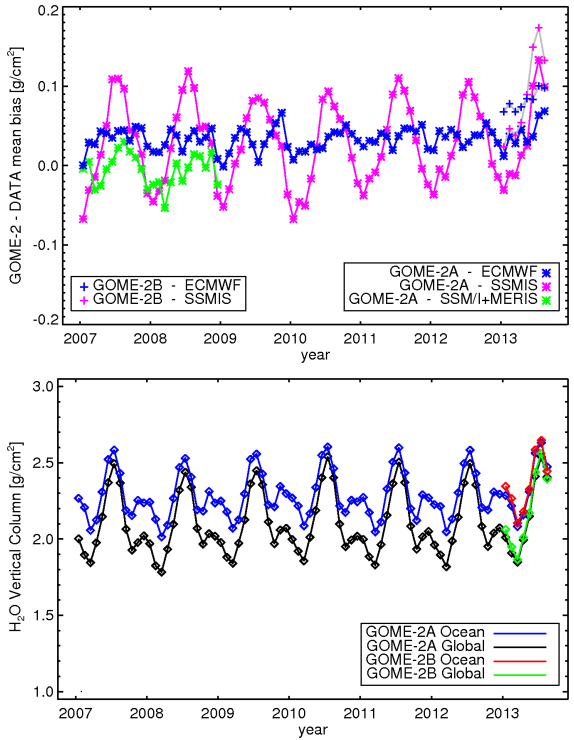

Fig. 7. Top panel: global monthly mean H_2O total column bias between GOME-2/MetOp-A and 3 independent data sets for the period January 2007–August 2013. The validation is performed against ECMWF ERA Interim reanalysis (blue points), SSMIS F16 satellite (magenta points) and combined SSM/I + MERIS data set (green points). The colored plus signs and grey lines show the bias between the most recent GOME-2/MetOp-B observations and the ECMWF and SSMIS data sets. Bottom panel: global monthly mean TCWV values for the GOME-2/MetOp-A and the GOME-2/MetOp-B data sets. The time series are computed for all surfaces (global: land and ocean together) and only for ocean measurements.

AMTD
7, 3021–3073, 2014

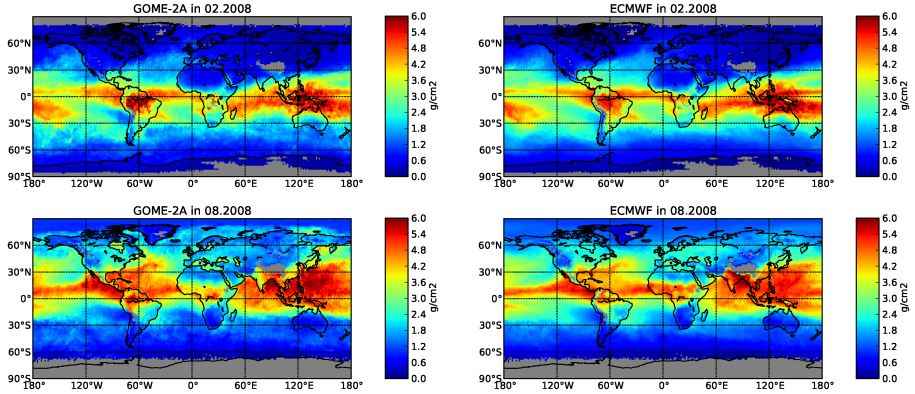

Fig. 8. Monthly mean maps of total column water vapour from GOME-2A (on the left) and ECMWF (on the right) co-located data for February 2008 (on the top) and August 2008 (on the bottom). Only cloud-screened data have been used.

AMTD
7, 3021–3073, 2014

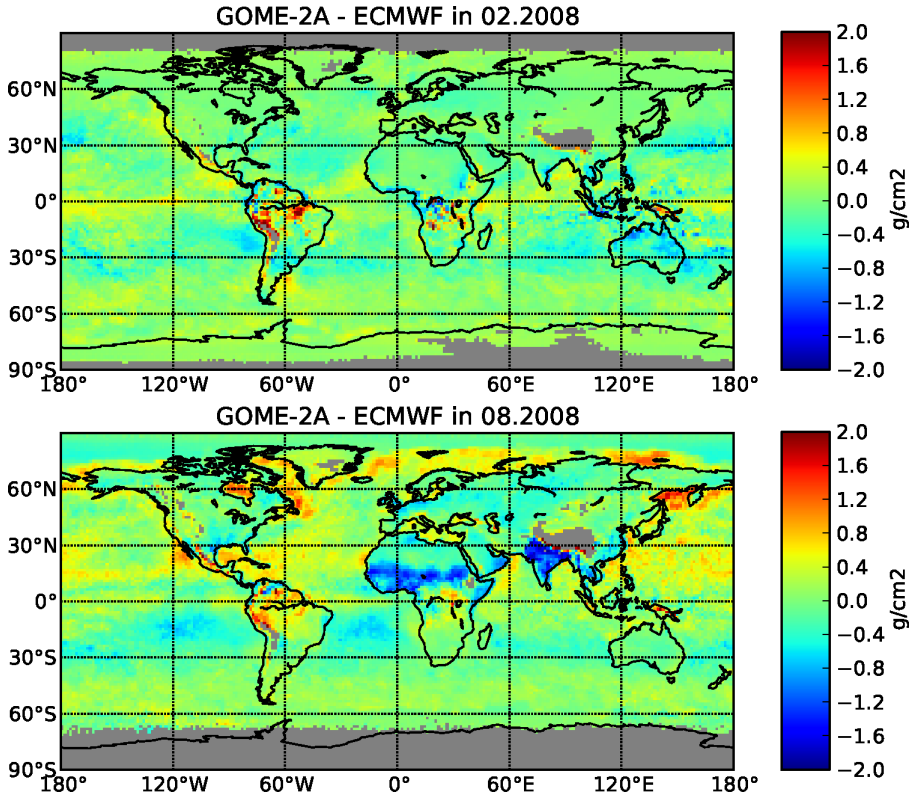

Fig. 9. Geographical distribution of the differences between GOME-2A and ECMWF water vapour column in February 2008 (top panel) and August 2008 (bottom panel). Only cloud-screened daily co-located data have been used.

AMTD
7, 3021–3073, 2014

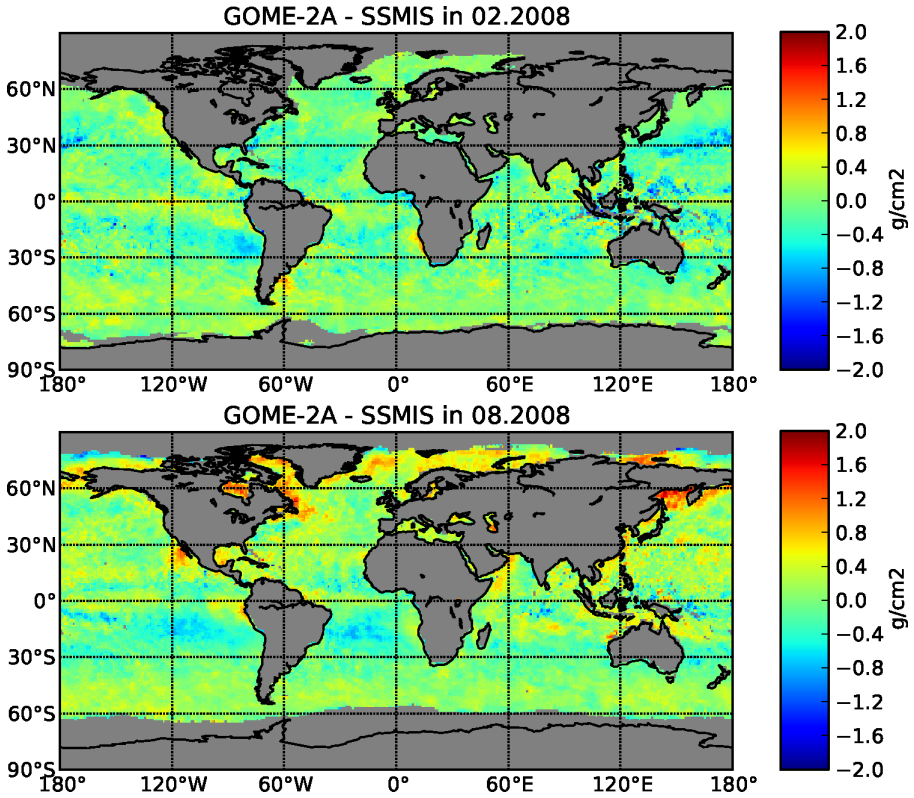

Fig. 10. Geographical distribution of the differences between GOME-2A and SSMIS water vapour column in February 2008 (top panel) and August 2008 (bottom panel). Only cloud-screened daily co-located data have been used.

AMTD
7, 3021–3073, 2014

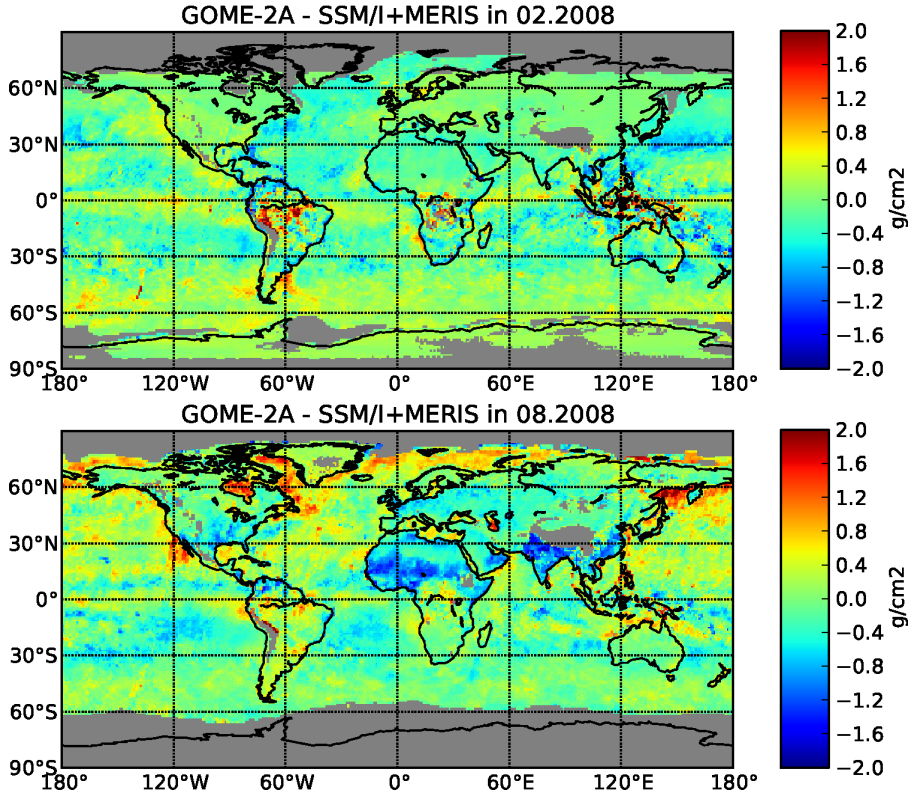

Fig. 11. Geographical distribution of the differences between GOME-2A and the combined SSM/I + MERIS water vapour column data set in February 2008 (top panel) and August 2008 (bottom panel). Only cloud-screened data have been used.

AMTD
7, 3021–3073, 2014

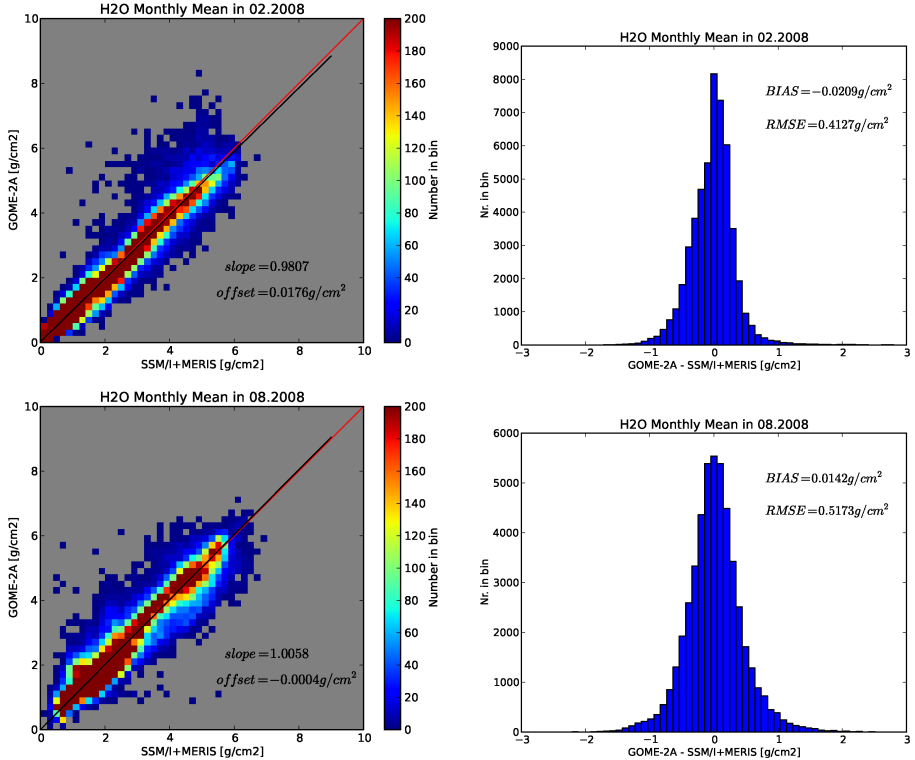

Fig. 12. Left top panel: scatter plot of GOME-2A monthly mean total columns against SSM/I + MERIS monthly mean total columns, for February 2008 (corresponding to Fig. 11, left panel). Cloud-free sky. Right top panel: histogram of the difference GOME-2A – GOME-2B, for the points in the scatter plot. Left and right bottom panels display the scatter plot and the histogram of the differences GOME-2A – SSM/I + MERIS for August 2008.

AMTD
7, 3021–3073, 2014